CHALMERS
UNIVERSITY OF TECHNOLOGY

A study of galaxy evolution: stacking emission lines from distant galaxies

JEAN-BAPTISTE JOLLY

Department of Space Earth and Environment
CHALMERS UNIVERSITY OF TECHNOLOGY
Gothenburg, Sweden 2019

Thesis for the degree of Licentiate of Engineering

A study of galaxy evolution: stacking emission lines from distant galaxies

Jean-Baptiste Jolly

CHALMERS
UNIVERSITY OF TECHNOLOGY

Department of Space Earth and Environment
Division of Astronomy and Plasma Physics
Chalmers University of Technology
Gothenburg, Sweden 2019

A study of galaxy evolution: stacking emission lines from distant galaxies

Jean-Baptiste Jolly

Division of Astronomy and Plasma Physics
Department of Space Earth and Environment
Chalmers University of Technology
SE-412 96 Gothenburg
Telephone +46 31 772 1000

Contact information:
Jean-Baptiste Jolly
Onsala Space Observatory
Chalmers University of Technology
SE–439 92 Onsala, Sweden

Phone: +46 (0)31 772 55 44
Email: jean.jolly@chalmers.se

Cover image: *This image from the NASA/ESA Hubble Space Telescope shows the galaxy cluster MACSJ0717.5+3745. This is one of six being studied by the Hubble Frontier Fields programme, which together have produced the deepest images of gravitational lensing ever made. Due to the huge mass of the cluster it is bending the light of background objects, acting as a magnifying lens. It is one of the most massive galaxy clusters known, and it is also the largest known gravitational lens. Of all of the galaxy clusters known and measured, MACS J0717 lenses the largest area of the sky.*
Credit: NASA, ESA and the HST Frontier Fields team (STScI)

Printed by Chalmers Reproservice
Gothenburg, Sweden 2019

A study of galaxy evolution: stacking emission lines from distant galaxies

Jean-Baptiste Jolly
Department of Space Earth and Environment
Chalmers University of Technology

Abstract

To draw up a thorough description of galaxy evolution exhaustive observations are needed, of distant but mainly of faint galaxies. Describing low mass galaxies is important to move the focus from the tip of the iceberg. While advances in telescopes capabilities have allowed to reach further galaxy, high-redshift studies are especially biased toward the brightest galaxies. In addition, well resolved spectral observations are needed to fully characterise the studied galaxies. Permitting the detection of emission or absorption lines, giving a direct access to galaxy composition. But spectral observations imply reducing further the signal to noise ratio (SNR), making line observations in faint high-redshift galaxies a difficult task.
Line stacking allows to get around intrinsic limitations in spectral observations, by averaging large galaxy samples, leading to drastic SNR improvement. However stacking, and especially line stacking, is not straightforward and requires a good handle of the population distribution, along with the output stack. To facilitate the use of such method, and to make data analysis tightly linked to stacking accessible, we produced an open source/open access tool, Line-Stacker.
After introducing the current state of knowledge on galaxy evolution, I will present Line-Stacker, describing both its main algorithm as well as the embedded data analysis tools. I will then introduce the two included papers and present their results. Paper I consists in a thorough description of Line-Stacker, and its test on numerous different simulated data-sets. Paper II is the first application of Line-Stacker on real data, in which we studied outflows from $z \sim 6$ quasars.

Keywords: Galaxies: evolution – Galaxies: high-redshift – methods: stacking – methods: data analysis – techniques: interferometric

Research Contributions

This thesis is based on the work contained in the following papers:

I Jolly, J. B., Knudsen, K. K., Stanley, F., Conway, J.:
LINE-STACKER: A spectral line stacking tool for interferometric data
Manuscript intended for Monthly Notices of the Royal Astronomical Society

II Stanley, F., Jolly, J. B., König, S., Knudsen, K. K.:
Outflows in $z \sim 6$ quasars
Submitted to Astronomy & Astrophysics

Acknowledgements

First, I would like to thank my supervisor, Kirsten, for her help and guidance, but also for giving me the chance to do this; for her trust and for the freedom she gave me, letting me explore the paths I wanted to take, while still keeping me on track. I would also like to thank Flora, whose help has been invaluable while writing this thesis and Paper I, and who was able to canalize my thoughts, providing the rigor, order and calm I sometimes lacked. A special thanks goes to Lucía, whose support and kindness allowed me to go through the writing phase. Finally I want to thank everyone at the SEE department (well, mostly people I know), especially from the division of Astronomy and Plasma Physics, for making these past years extremely enjoyable!

Jean-Baptiste Jolly, Gothenburg, February 2019

This too shall pass.

CONTENTS

CHAPTER 1

INTRODUCTION

1.1 From the big bang to the dark ages

The Universe as we see it today is mostly empty, and most of its energy content is invisible. The total baryonic matter accounts for only 4.5% of the total energy, from which less than 10% (0.3% of the total energy) lies in the visible matter, such as stars in galaxies, hot gas in clusters and groups of galaxies. Aside from baryonic matter, the universe is thought to consist of dark matter (24%) and dark energy (71.5%), both being mostly unknown (Persic and Salucci, 1992). But the observable universe used to look very differently.

Modern cosmology describes the Universe as starting from the big bang[1], marking the beginning of time. At that moment the universe is extremely dense but starts expanding rapidly, becoming sparser[2]. Because it is very complicated, still largely debated and definitely not the scope of this work, we are going to skip the first seconds after the big bang, to start our story just around the first minute (see e.g. Tanabashi et al., 2018, for an extensive description of the very early universe).

At this time the universe is still very dense, composed mainly of high energy photons, created primarily through matter/antimatter annihilation. As the universe keeps on expanding, the energy density diminishes, the mean free path of photons gets bigger and, after 2 minutes, the energy density is sufficiently low for the first nucleus to be stable. However, the energy density is still high, and the high energy photons break apart newly formed nuclei. Consequently only a handful of nuclides species are allowed to be formed (mainly protium, deuterium and helium-3 and 4). As energy density gets lower, and mean free path of particles increases, recombination becomes possible: electrons are captured by nuclei, forming the first neutral atoms. Because recombination directly to the ground state is very inefficient, electrons are typically captured in higher states, and later drop to the lower states, releasing photons in the process. This phenomena is know as photon decoupling

[1] See Figure 1.1 for a graphical guide to the following description.

[2] It is worth noting that, unlike the common appreciation, if the universe is infinite now (and that we cannot say for sure) it was infinite already "when" the big bang happened.

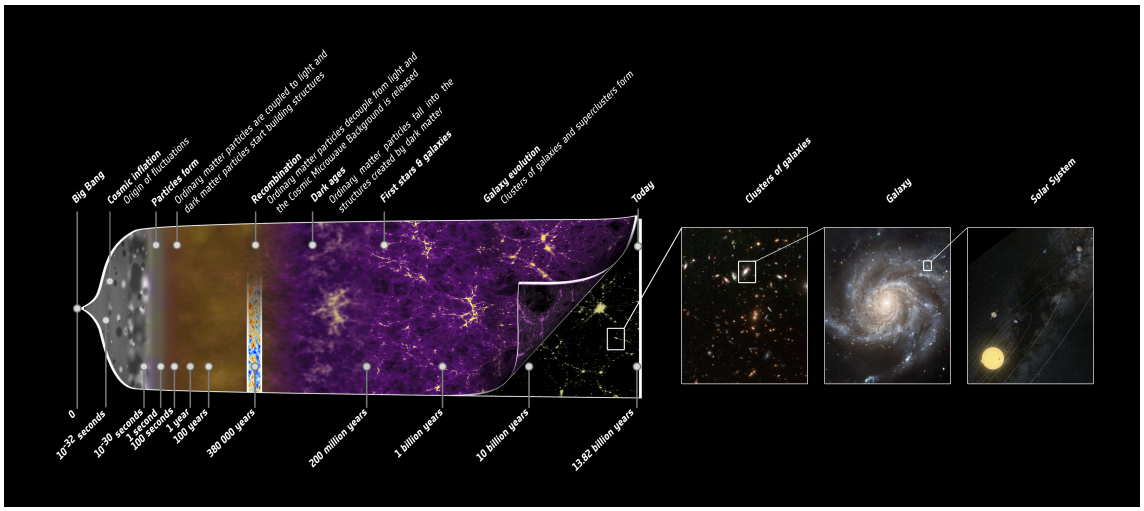

Figure 1.1: History of the universe ©ESA – C. Carreau

(see e.g. Coc and Vangioni, 2017; Tanabashi et al., 2018).

All these photons start travelling freely for the first time since the big bang, they are "the first light of the universe". They constitute the Cosmic Microwave Background (CMB), which was first detected by Penzias and Wilson in 1964, and most recently studied by the satellite Planck, launched in 2009 (see Planck Collaboration, 2016). Planck's very sensitive observations allowed to show the existence of a preferred correlation scale, printed on the CMB fluctuations, translating, on large scale structures, to a distance of 100-150 Mpc. Later, SDSS observations showed that this distance matched the observed correlation scale for galaxies in the near universe (Okumura et al., 2008). Showcasing the relation between inhomogeneities in the particle soup of the early universe and large scale structures thousands of light years big in the present universe, hence connecting small scales to big scales, past to present, the big-bang to galaxies.

After decoupling there is almost no new source of photon in the universe for over 100 million years. The creation of stars, and furthermore of galaxies, takes time in an almost perfectly homogeneous universe. Because this epoch exhibits almost no light creation it is called "the dark ages". Due to lack of photons, there is almost no information about this period, and it is today one of the hardest task of astronomy to try and find objects (stars, galaxies), first of their kind, in the dark ages.

1.2 From the first galaxies to the local Universe

During the dark ages, on a large scale, dark matter gathers forming filaments, assembling in a dark matter network (see Figure 1.2). Normal matter, which is mostly in the form of gas at that point, is in higher density at the nodes of the dark matter network. In these dense matter cores, while the temperature is still too high to allow structure formation of normal matter, cold dark matter gravitationally collapses, starting from small inhomogeneities and growing linearly by accretion. Eventually these dark matter clumps reach critical density and collapse, creating the first dark

matter halos. These halos grow either through accretion or by merging. Ultimately they will act as attractors for the normal matter, allowing it to bound into structures earlier than it would have been possible otherwise.

The first stars form, and bound together through gravity, forming the first galaxies. The stars and galaxies are a new source of radiation, and the photons they emit interact with the neutral hydrogen atoms in the gas surrounding them, stripping them out of their electron and making the whole universe ionized again. This process is referred to as reionization. The universe becomes bright, it is the end of the dark ages.

From this point on, bigger galaxies start forming, by accreting matter and/or through merging, and the universe looks essentially the same as it does now. However, galaxy growth is not homogeneous: most massive galaxies are formed very fast while smaller clumps take a long time to evolve. Leading to the whole zoo of galaxy classes that we observe today. Coming in all sizes and shapes, some displaying strong, ongoing, star formation while other appearing to have been passive for a while. Similarly, some galaxies are gas rich, displaying many different chemical species, while other seem mainly metal poor. The evolutionary path leading to such differences is still unclear, and the complete picture of galaxy evolution is yet to be drawn.

1.3 This thesis

The present Licentiate thesis is in the topic of galaxy formation and evolution. The number of galaxies in the observable universe is estimated to above hundred billions. With the growing number of sensitive telescopes, our knowledge of galaxy evolution is gradually increasing. But even with new and better telescopes there remains many scientific questions, especially because, while better instruments allow us to see further, these observations remain biased toward the brightest objects, preventing us to draw up a complete picture of galaxy evolution, taking into account even the fainter individuals. The scope of this work is to present a newly developed tool, Line-Stacker, which aims to enable broader investigations of distant galaxies, more especially by studying their gas content. Through stacking a large number of sources, the signal to noise ratio (SNR) can be drastically improved, enabling to study faint emission, thus highlighting otherwise invisible galaxy properties. In the following chapters I broadly introduce the current state of knowledge in the field of galaxy evolution before presenting the developed tool, Line-Stacker, itself. I then describe the aim and content of the two embedded papers, followed by the potential outlooks to this work, both in terms of methodology and scientific projects.

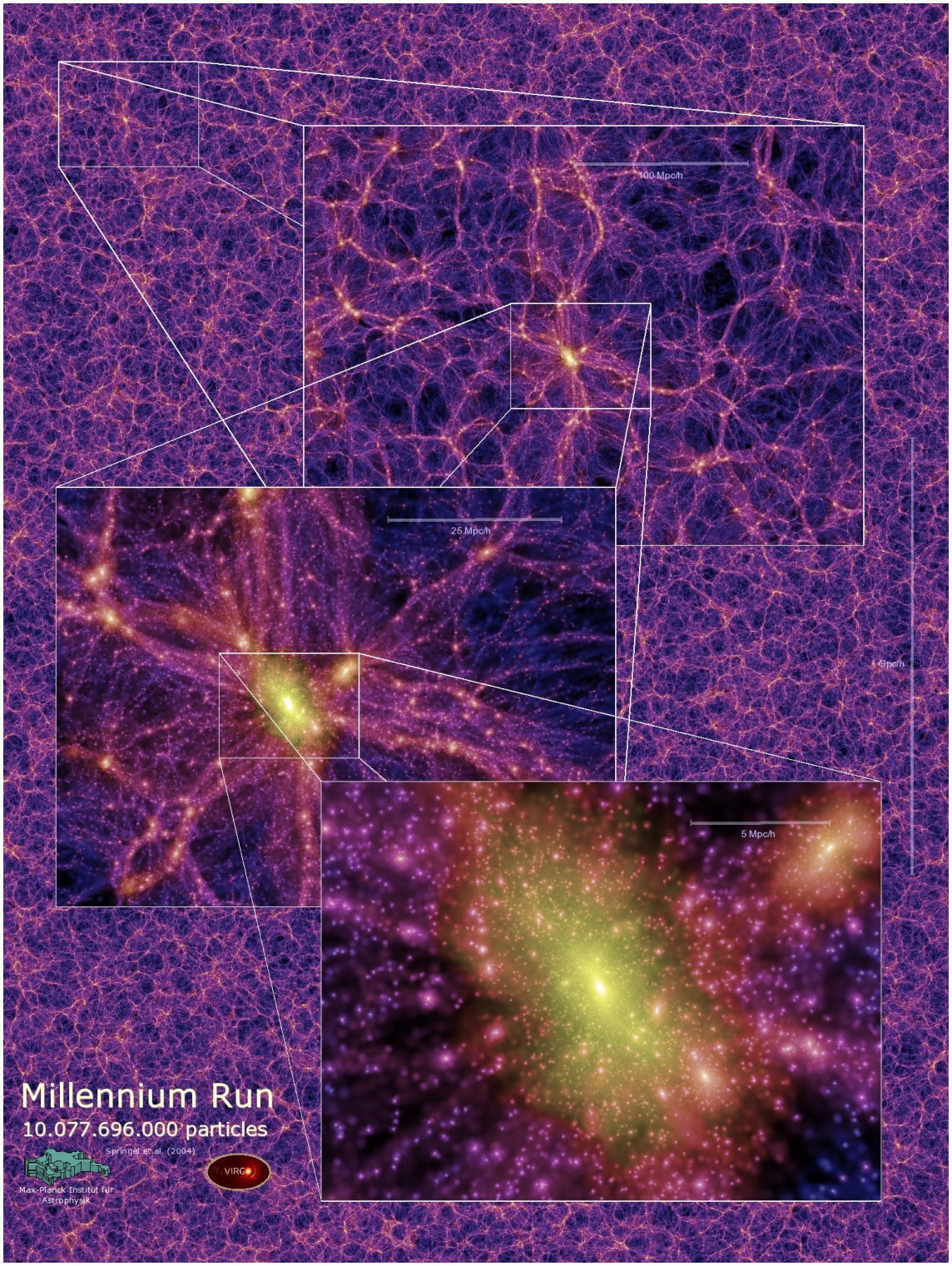

Figure 1.2: ©Millenium simulation: *Slices of the dark matter distribution. The following poster shows a projected density field for a 15 Mpc/h thick slice of the redshift z=0 output. The overlaid panels zoom in by factors of 4 in each case, enlarging the regions indicated by the white squares.*

CHAPTER 2

GALAXY EVOLUTION

2.1 Growth process

About a hundred years ago, the 'Great debate' focused on whether the Milky Way essentially represented the whole universe, or if it was one galaxy among many others. It was resolved through the distance measurements to the Andromeda galaxy, showing that it was too far away to be part of the Milky Way. From this time it was known that we lived in one galaxy among others, leading to new studies of external galaxies, and to the birth of extragalactic research. Among the first important steps was the classification of galaxies. The most common classification is the Hubble classification scheme, separating galaxies into four categories, elliptical, lenticular, spirals, and irregulars (see Figure 2.1). Elliptical and lenticular are usually referred to as "early type galaxies" while spirals and irregular are referred to as "late type galaxies"[1].

Galaxies exhibit a wide variety in characteristics such as size, mass and color. For example, galaxy stellar masses span a large range, over more than seven order of magnitude. The least massive (dwarf) galaxy detected (Kirby et al., 2013) having a (stellar) mass of $\sim 10^5\,M_\odot$, while one of the most massive galaxy detected has a (total) mass of $\sim 10^{13}\,M_\odot$ (Carrasco et al., 2010, ten times more massive than the Milky Way). However the first big structures to form were likely star clusters, group of stars, gravitationally bound (White and Rees, 1978). Thus the question: how did galaxies grow from the earliest phases to the structures we see day, in such a wide variety as described by the Hubble sequence. There are two major processes for galaxy growth: accretion of matter and merging.

[1]It should be noted that the terms "early" and "late" do not refer to temporal evolution. It is sometimes thought that Hubble intended this temporal relation, and that it was later disproved. But, as explained in Baldry (2008), Hubble borrowed this vocabulary from star classification and, as he wrote in his 1926 paper: *"Early and late, in spite of their temporal connotations, appear to be the most convenient adjectives for describing relative positions in the sequence... They can be assumed to express a progression from simple to complex forms."*.

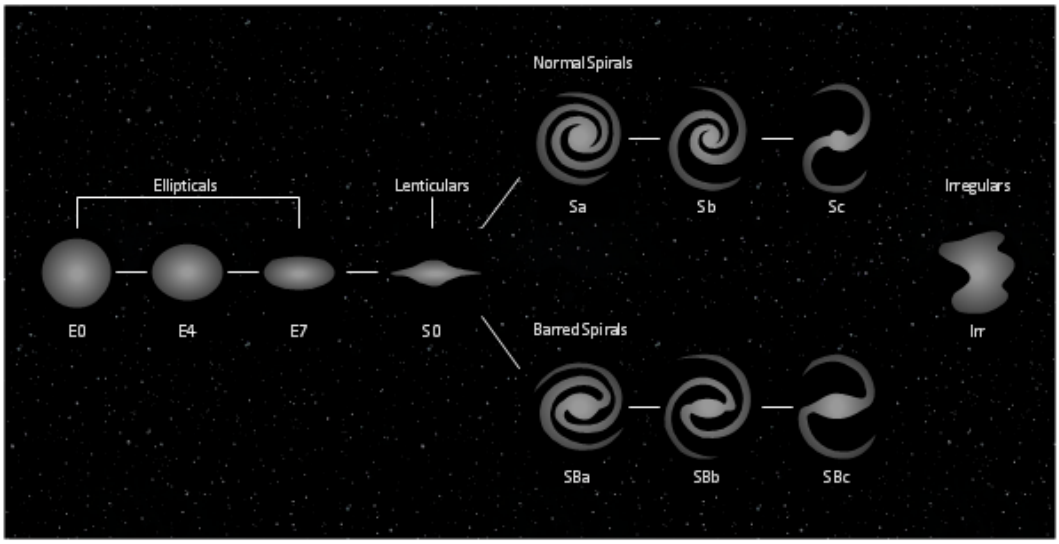

Figure 2.1: Hubble sequence: galaxy classification.

2.1.1 Accretion

Accretion of matter is facilitated by the dark matter network (as illustrated by Figure 1.2). Gas flows through the dark matter web, and is accumulated at the nodes. Galaxies are usually formed along the filaments, with the most massive at their intersections (e.g. Springel et al., 2005; Vogelsberger et al., 2014). The gas flowing through the web is accreted by the galaxies, thus growing their mass. There are two main modes of accretion: the hot and cold modes (e.g. Katz et al., 2003; Kereš et al., 2005). One of the main issues with accretion is that the accreted gas must be at sufficiently low temperature to be captured by the galaxy. Hot mode accretion implies that the infalling gas is hot (meaning $T_{gas} > T_{virial}$), due to shock heating, and must thus cool, mainly through radiation, before it can be integrated in the galaxy. The hot mode is quasi-spherical and dominates at lower redshifts ($z < 1$) in high density environment. In the cold mode, the accreted gas is channeled along the filaments, allowing galaxies to draw gas from large distances. The gas is still heated, from shocks and adiabatic compression, but it radiates its heat just as quickly, so that its temperature never reaches T_{virial}. Cold mode is dominant at high redshifts and in low density environments at $z \sim 0$ (e.g. Kereš et al., 2005; Dekel et al., 2009).

2.1.2 Galaxy merger

Galaxy mergers consist in combining two (or more) galaxies together to form a bigger one (see Figure 2.2). When it comes to growing galaxies we distinguish between 3 modes, depending on the mass ratio of the two galaxies merging (M_r): "major" if $M_r > 1/3$, "intermediate" if $1/3 > M_r > 1/10$ and "minor" if $M_r < 1/10$.

When two galaxies of similar masses merge, the forces involved are such that their dynamic structure is lost after the merging (Barnes and Hernquist, 1996). For this reason it is thought that elliptical galaxies are the product of major merging

events. As an example, our galaxy, the Milky Way, and the Andromeda galaxy are gravitationally bound and modelling suggests that they will eventually merge, in roughly 4 billion years (van der Marel et al., 2012). Being of similar mass (ratio 1/1.5) this will be a major merging event and their global dynamic structure will hence most probably be lost. On the other hand, minor and intermediate mergers should leave the structure of the most massive galaxy intact, being hence one of the possible process behind the growth of massive spiral galaxies (Naab et al., 2009). It is thought that our own galaxy grew, and is still growing today, through the absorption of the Canis Major Dwarf Galaxy and several other smaller systems (Martin et al., 2004).

Additionally, merger events can also be classified depending on the gas richness of the galaxies involved. If the galaxies are gas-rich the merger event is classified as a "wet merger". Conversely, if both galaxies are gas poor the event is classified as "dry merger". The term "mixed merger" is an intermediate mode, when one galaxy is gas rich and the other gas poor. Wet mergers seem to dominate at higher redshift, but the higher number of dry mergers at lower redshift may simply correlate with the increasing number of gas poor galaxies with reducing redshift (Lin et al., 2008). Gas-rich major mergers trigger starburst in the early phase, followed by rapid black hole growth through gas inflow to the center (e.g. review by Sanders and Mirabel, 1996). It is thought that such events may be, at least in part, responsible for the observed quasar population, with >75% of the red quasars population showing evidence of recent/ongoing merging, decaying ultimately into a passive elliptical state (Hopkins et al., 2006, 2007). However, the frequency evolution of mergers with redshift is still debated (e.g. Bertone and Conselice, 2009; Le Fèvre et al., 2013; Rodriguez-Gomez et al., 2015).

2.2 Observing high-redshift galaxies

In 1995 extensive observations with the *Hubble Space Telescope* resulted in the release of the *Hubble Deep Field* (see Figure 2.3), first of its kind, this extremely deep image showed a high number of galaxies. New galaxy classifications arose, based on observed physical properties instead of solely on morphology. Around the year 2000 identifications of distant galaxies were typically made through observation of extremes objects, mostly quasars, rest frame UV-bright Lyman-break galaxies (Steidel et al., 1996) or extremely red objects (Daddi et al., 2000). Later new methods have been developed to identify weaker galaxies, like dust-obscured galaxies (Dey et al., 2008), distant red galaxies (Franx et al., 2003) or BzK galaxies (Daddi et al., 2004).

As the timescale of galaxy evolution is much longer than our life time, it is not possible to follow the evolution of an individual galaxy. Methods mentioned above allow identification of galaxies holding specific characteristics, but since these methods are intrinsically very different, and operate in different frequency ranges, it is challenging to link galaxy types together. One of the biggest challenges is hence to tell if these classes represent different stages of galaxy evolution or if they are simply different populations that have evolved separately. To establish evolutionary links it is important to have multi-wavelength observations, as observing in different

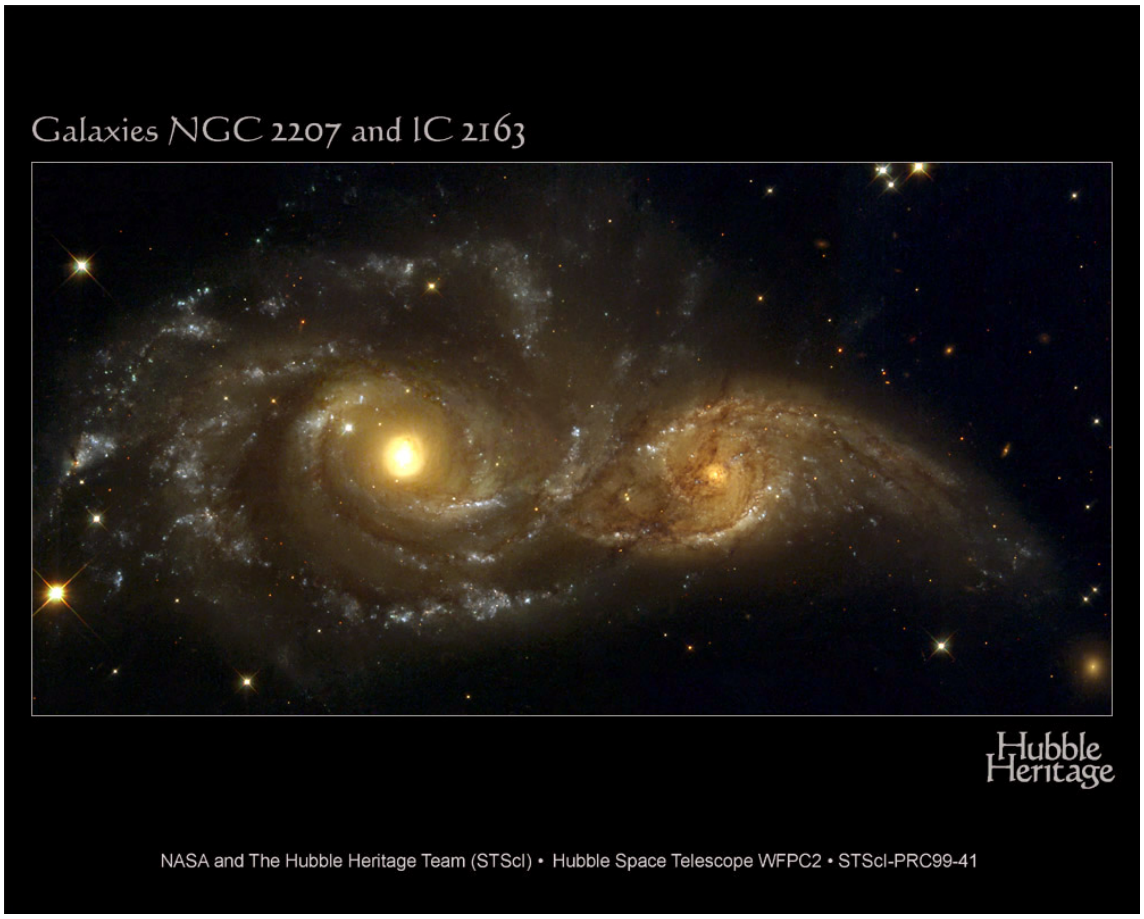

Figure 2.2: The merging of two spiral galaxies.

spectral windows allows to fully classify a given galaxy. Additionally, a given object can be bright in a given wavelength range while faint in an other, and, wavelengths getting shifted with redshift, this is an additional reason for a multi-wavelength description to be absolutely needed to observe galaxies across redshifts.

Because observed flux goes down as the square root of the distance to the emitting object, observed distant galaxies often have very high intrinsic luminosity. But high luminosity objects at high redshift really represent only the tip of the iceberg: a small, extreme, part of the galaxy population. Making an extensive description of high-redshift galaxy populations even harder. Linked to this is the Malmquist bias, leading to an overestimate of the average brightness of distant galaxies, inducing a miss-interpretation of the brightness level of the studied sample, compared to the average population.

2.3 Observational probes of the gas content in distant galaxies

One key aspect of understanding galaxy evolution is the study of the evolution of the gas content through time. The interstellar medium (ISM) of star-forming galaxies contains the gas that fuels the star formation, as well as the processed gas that

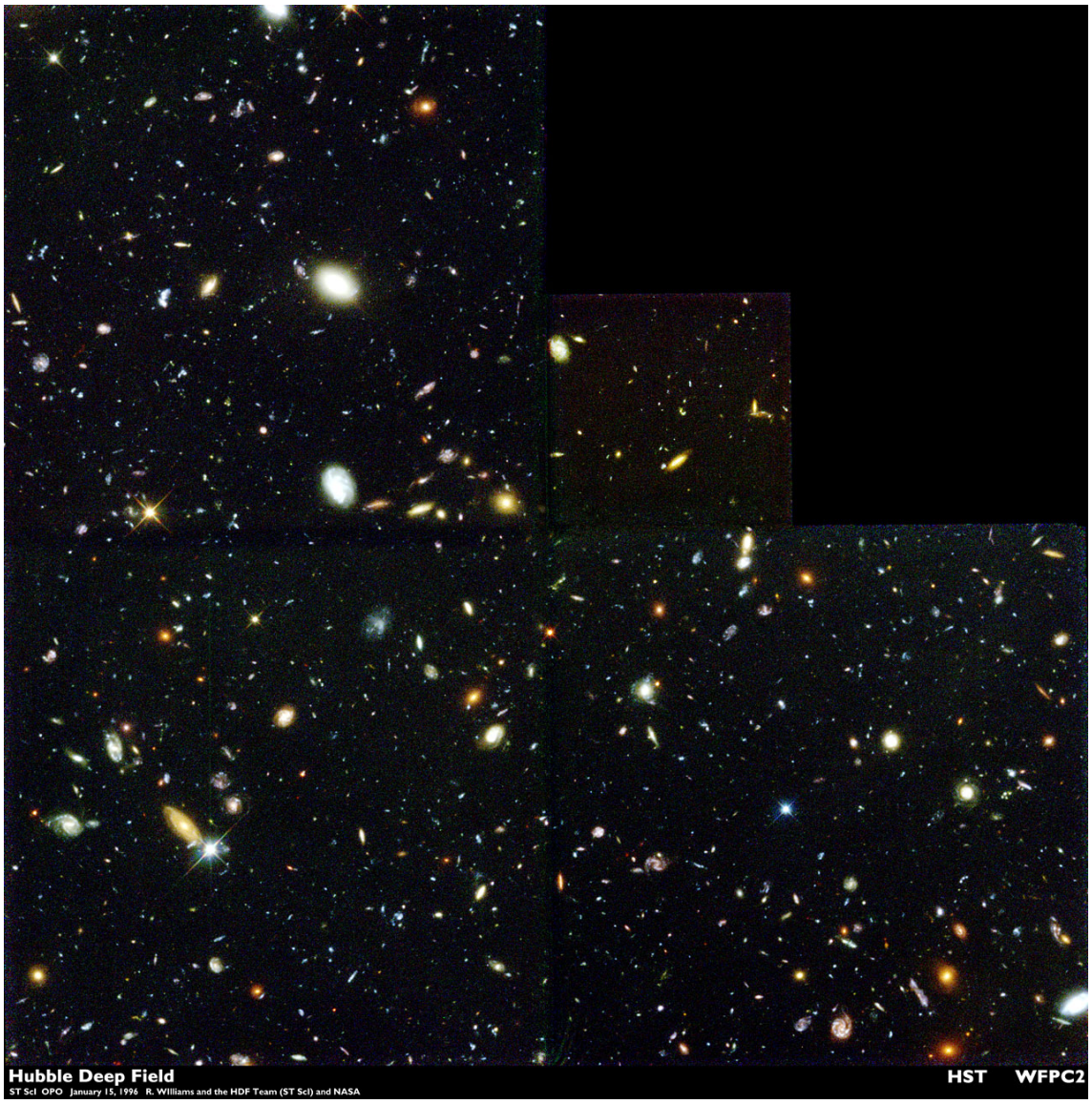

Figure 2.3: The Hubble Deep Field

comes from stellar evolution. There are two different gas phases in the ISM: neutral and ionized, that often have a wide range of temperature and density. The neutral phase is dominated by the neutral atomic and molecular gas, as well as by the dust content. This phase is both found as diffuse gas, and in molecular clouds that can be the sites of star formation. The ionized phase is typically dominated by the ionized atomic gas with a very low content of molecules and dust. This gas can be found near young OB stars or in the diffuse medium.

Thorough studies can reveal chemical composition of galaxies (e.g Costagliola et al., 2015; Henkel et al., 2018), and being able to map the evolution of galaxy composition through the ages would be a huge step in understanding galaxy formation, and the evolution of our own Milky Way. By studying the different atomic and molecular emission lines, it is possible to investigate the physical and chemical properties of the gas. The most common emission lines are (non-exhaustive list,

focused on the radio/mm/far-infrared):

- The atomic hydrogen HI 21 cm line, it probes the large gas reservoir in galaxies, it is mostly optically thin, allowing easier total mass calculation (e.g. Walter et al., 2008) and hence gas/stellar mass fraction estimate (e.g. Zwaan et al., 2013). It can also possibly trace the streams growing galaxies – Cold Mode Accretion, see section 2.1.1 (e.g. Morganti et al., 2006). But HI observations at high redshift are very challenging because they require a high sensitivity.
- Atomic fine-structure lines in far-infrared probe different parts of the ISM. For examples, the [C II] 1900 GHz line is known to be one of the strongest cooling line in the ISM, and one of the brightest emission lines from star forming galaxies (e.g. Smith et al., 2017; Lagache et al., 2018). The neutral carbon lines [C I] traces physical and chemical conditions of the dense ISM (e.g. Stutzki et al., 1997), it has also been shown to trace molecular gas, acting as an alternative to CO (Clark et al., 2018). The ionized oxygen [O III] at 88 μm is a known tracer of activity in galaxy nucleus (e.g. Kauffmann et al., 2003), as well as a good tracer of metal in galaxies (e.g. Pettini and Pagel, 2004).
- A large number of molecules: H_2, molecular hydrogen, is the most abundant molecule by far, with only around 1% of the gas in other molecules. But H_2 has no permanent dipole moment and is therefore difficult to observe (e.g. Tielens, 2005). CO is the second most abundant molecule and is very easy to observe because its lowest excited level is around 5.5 K and is thus very easy to excite, making the rotational transitions of CO the most common emission lines observed in high-redshift galaxy studies. CO is hence used as a tracer of H_2 (e.g. review by Carilli and Walter, 2013; Lagos et al., 2014). CO traces primarily gas with moderate density, and has been shown to trace star formation rate (e.g. Omont, 2007). There is, however, many more molecules that are of interest for galaxy evolution studies, e.g. the high gas density tracers HCN and HCO^+, or the water lines that have so far only been studied in a few sources.
- Dust is observed through absorption of the blue to UV radiation which is then re-emitted and observed at far-infrared and millimeter wavelengths. ISM properties can be deduced from dust observations (see Scoville et al., 2014), and dust has been observed in galaxies at redshift as high as $z \sim 7.5$ (Knudsen et al., 2017).

All these can typically be detected through emission/absorption lines observations. But such investigation are much harder than continuum observations: when looking for lines, one has to have a good sensitivity individually on many spectral channels, while continuum allows to sum all these channels together, hence recovering a higher SNR.

2.4 AGN & outflows

Starting from the 1980's numerous studies detected super-massive black holes in the center of galaxies (e.g. Sargent et al., 1978; Dressler and Richstone, 1988; Harms et al., 1994), and it is now widely accepted that all massive galaxies contain a central super-massive black hole. In parallel, the presence of extreme optical/radio

phenomenon in some galaxies was attributed to the mechanism of mass accretion onto a black hole (e.g. review by Rees, 1984; Lynden-Bell, 1969). These extreme sources are now known as active galactic nuclei (AGN).

By studying super-massive black holes, and their relation to their host galaxy, it was shown that there exists a proportionality between black hole mass and mass of the galactic bulge (e.g. Marconi and Hunt, 2003; Häring and Rix, 2004). Such a relation could be explained by the process known as AGN feedback. Both black hole growth and star formation require cold gas, however, while black holes only accrete gas on small scales ($< 1\,\mathrm{pc}$) star formation operates on galactic scales. Thus, how to expend the influence of AGN by a factor $\sim 10^5$? While still debated, many studies propose that AGN would act on the cold gas through violent outflows: either warming the gas up or mainly expelling it out of the host galaxy, hence quenching star formation (e.g. reviews by Fabian, 2012; Alexander and Hickox, 2012). Furthermore, simulations of galaxy formation show that a quenching process from AGN feedback allowed to properly reconstruct galaxy stellar mass functions that would otherwise be over-estimated (e.g. Di Matteo et al., 2005; Somerville et al., 2008; Schaye et al., 2015) (review by Naab and Ostriker, 2017).

While outflows have been observed in massive low redshifts galaxies (e.g. Rupke and Veilleux, 2011; Maiolino et al., 2012; Cicone et al., 2014; Harrison et al., 2014) there has been but a few observations at higher redshifts (e.g. Cicone, 2015; Decarli et al., 2018), and mainly targeting sources with a high chances to be in an outflowing phase (Circosta et al., 2018). Furthermore, as shown in Harrison et al. (2018), deriving outflow properties (such as mass, extent, velocity etc.) is a hard process, more especially to link to AGN luminosity. Hence, using current observations, one cannot draw a definitive conclusion regarding the outflows' rate across redshift. Especially, on whether outflows is a common process, or limited to a certain galaxy-mass range or redshift range, hence questioning the role of AGN feedback in the global picture of galaxy evolution. While studies like Circosta et al. (2018), targeting blindly detected sources at $z \sim$2-3, are an important step toward generalizing outflow properties, studies like the one described in Paper II, allow for unbiased statistical analysis of high redshift AGN.

2.5 Open questions

While both merging and accretion processes are mostly accepted as responsible of galaxy growth many questions remain. For example the respective distribution of both processes across redshifts remains unclear. Similarly, the relation between the super-massive black hole at the center of galaxies and the properties of the galaxy itself is still questioned, in particular the role of feedback processes from AGN in the early universe and their consequence on star formation. In a broader view, the star formation evolution across ages, and the mechanism allowing star formation to be switched on or off, as well as its fueling, are still investigated. Additionally the content of galaxies: the nature and amount of gas, available at different stages of galaxy evolution is not well described by current theories. The role of the environment on galaxy formation, as well as the galaxy population distribution as a function of the redshift are still questioned. Current observations do not permit

for a broad enough, global view, that would allow to draw up a general description of, and properly diagnose, galaxy evolution across ages.

CHAPTER 3

RADIO INTERFEROMETRY

3.1 Introduction to interferometry

The main purpose of interferometry is to significantly improve angular resolution. A standard two-element interferometer functions by studying, not directly the signal received from the source, but the correlation between the outputs of two antenna systems. The outputs are superposed, creating interference that can be studied to retrieve information about the original signal, emitted by the source. In order to improve the limited performance of a two-element interferometer, "aperture synthesis" is done by using an array of antennas. For a single dish the resolution, R, is inverse proportional to the size of the dish, $R \propto \lambda/D$, where λ is the wavelength of observation and D the antenna dish diameter. In an interferometer the resolution is $R \propto \lambda/L$ where L is the maximal distance between antennas in the array ($L >> D$, hence largely improving the resolution of interferometers compared to single dish observations). Aperture synthesis works by correlating the outputs of each antenna pair in the array. Every antenna measures the power of incoming signal over time, and the so-called visibilities are the measure of the coherence of the signal. The visibilities, $V_{j,k}(t)$, for antennas j and k at time t are linked to both the source brightness, I, and the distance between the antenna pair, $\vec{B}_{j,k}$:

$$V_{j,k}(t) \propto \int_{sky} I(\vec{\sigma}) e^{\frac{-2i\pi}{\lambda}\vec{B}_{j,k}\cdot\vec{\sigma}} d\Omega \tag{3.1}$$

Where $\vec{\sigma}$ is the vector describing the position on the sky. Visibilities are usually expressed in terms of (u, v), defined as:

$$\vec{B}_{j,k} \cdot \vec{\sigma} = \lambda(ul + vm) \tag{3.2}$$

where (l, m) is the coordinate system used to describe $\vec{\sigma}$. Allowing to rewrite 3.1 as a 2D Fourier transform:

$$V_{u,v} \propto \int_{sky} I(l, m) e^{2i\pi(ul+vm)} dldm \tag{3.3}$$

However, because the number of antennas is not infinite, there is a limited number of antenna pairs ($N \times (N-1)$ where N is the total number of antennas), and hence a limited number of $\vec{B}$, which leads to a discrete spanning of the visibility space.

The combination of all (u, v) points sampled by the array configuration is referred to as *uv*-coverage (see Figure 3.1). Because there cannot exist a null distance between antennas, the point $u = v = 0$ is not probed[1]. Furthermore, a whole area in the center of the *uv*-plane, corresponding to distances smaller than the shortest baseline, remains un-sampled. This means that extended emission will be, to some extent, lost when using interferometers. Similarly, the largest baseline will determine the maximum achievable resolution by the interferometer. Because the Earth rotates, the *uv*-coverage changes as time passes, hence longer observations allow for a more complete coverage of the *uv*-plane (see Figure 3.1). Because of the under-sampling, using proper (inverse) Fourier transform is not a possibility to go from the *uv*-plane to the image-plane. The most popular method to image visibilities is the so-called clean algorithm first developed in Högbom (1974). However, it is important to note that visibilities are the actual data, images are model representations of this data, and, as such, they are model dependent. The algorithm used to image the visibilities could significantly affect the produced images. This is especially true for low SNR data, where artifacts (such as dirty beam) will be hard to remove when imaging.

3.2 Radio interferometers

There is a growing number of radio and millimeter interferometric arrays. Bellow we describe the two probably most prolific: The Atacama Large Millimeter/submillimeter Array (ALMA) and The Karl G. Jansky Very Large Array (VLA). But there are many other, e.g. the Submillimeter Array (SMA), the Low-Frequency Array (LOFAR), the Australia Telescope Compact Array (ATCA), the IRAM NOrthern Extended Millimeter Array (NOEMA). Among the new generation are MeerKAT and ASKAP (Australian Square Kilometre Array Pathfinder), which are the pathfinders for the future SKA, which will be the biggest radio interferometer, expected to be operating in 2028. Furthermore, radio interferometry is done at many scales, with for example the use of VLBI (Very Long Baseline Interferometry) techniques, allowing to have baselines basically the size of the Earth.

3.2.1 Atacama Large Millimeter/submillimeter Array (ALMA)

ALMA is an astronomical interferometer composed of 66 antennas. It is located in the Atacama desert in Chile, at $\sim 5000\,\mathrm{m}$ elevation. Its construction began in 2004 and it is a joined ESO (European Southern Observatory), NRAO (National Radio Astronomy Observatory), NAOJ (National Astronomical Observatory of Japan) and Chile project. The location was chosen because it is one of the highest and

[1] The central region in the *uv*-coverage can be filled in with a so-called "zero-spacing" observation: by using a single dish telescope to recover large angular scale information.

driest place on Earth, minimizing the effect water vapor has on observations. As its name indicates observations are carried out in the millimeter/submillimeter range, from 0.32 mm to 3.6 mm. The antennas are separated in 2 arrays: the main array, consisting of fifty 12 meter diameter antennas, and the Atacama Compact Array (ACA) composed of four 12 meter and twelve 7 meter diameter antennas. One of the impressive technological feat is that antennas can be moved (on trucks), allowing the array to assume different configurations: permitting distances between antennas from 150 m to 16 km. Being able to move antennas, and to change the distance between them, allows for different *uv*-coverage, some being more suited for specific observations. For example, longer baselines configurations will lead to better spatial resolution, while shorter ones will be favored for large scale observations because improving the field of view. ALMA's spatial resolution is up to 10 milliarcseconds which is five times better than the Hubble Space Telescope, and its spectral resolution is up to $50\,\mathrm{m\,s^{-1}}$. ALMA has been operating since late 2011, lead to publications of more than 1000 scientific papers (reaching 1000 in June 2018) in many different area of astronomy, from smaller scales, with studies of the sun, to very distant observations, investigating for example early galaxy formation.

3.2.2 Karl G. Jansky Very Large Array (VLA)

VLA is an astronomical interferometer composed of 27 antennas. It is located in the United States of America, in the state of New Mexico at $\sim$2100 m elevation. Its first observation took place in 1980 but the array was upgraded in 2011, changing its name from the former "Very Large Array" to the actual "Karl G. Jansky Very Large Array", and upgrading its overall capacities by a factor 8000. Each of the VLA's antennas have a diameter of 25 meters and are positioned to form "Y" shape (see Figure 3.1). Antennas can be moved along rails, resulting in 4 different possible configurations (depending on the baseline's length). The most compact configuration (configuration D) shows a maximum baseline of 1.03 km and a minimum baseline of 35 m, corresponding to a resolution of 7.2 arcsec and a field of view of 145 arcsec. The most expanded (configuration A) shows a maximum baseline of 36.4 km and a minimum baseline of 680 m, corresponding t o a resolution of 0.2 arcsec and a field of view of 5.3 arcsec. The frequency coverage is 74 MHz to 50 GHz. Similarly to ALMA, VLA is used in basically all fields of astronomy.

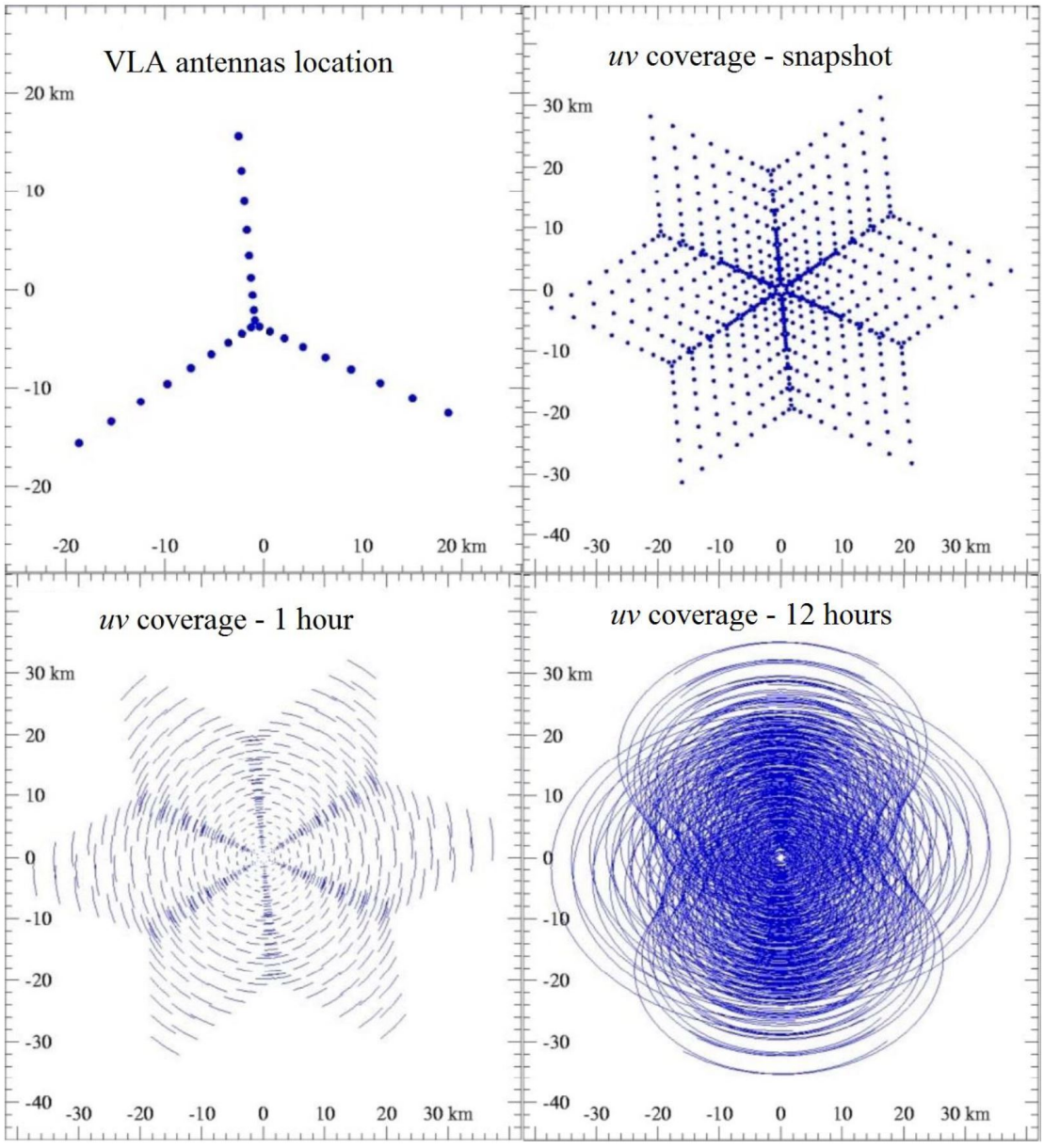

Figure 3.1: VLA antennas location and *uv* coverage: as a snapshot, after 1 hour, after 12 hours.

Figure 3.2: ALMA: aerial view of the antennas located in the Central Cluster, in their construction stage.

CHAPTER 4

LINE-STACKER

Observing high-redshift galaxies is an extremely complex task, more especially when trying to identify emission lines from low mass systems. About two days of ALMA integration time would be needed to detect a $z = 2.5$ CO(4-3) line of luminosity $L'_{\rm CO} = 10^9\,{\rm K\,km\,s^{-1}\,pc^2}$, which corresponds to a galaxy with gas mass about few times $10^9\,{\rm M_\odot}$. In contrast, a galaxy 10 times more massive would only require 37 minutes on source. Similarly, to detect a [C II] line, with a width of $200\,{\rm km\,s^{-1}}$, coming from a galaxy at $z = 6$, with a star formation rate of $\sim 10\,{\rm M_\odot\,year^{-1}}$, would require an ALMA integration time of ~ 6 hours. And that is to observe one single source. Many more similar observations would be needed to draw a statistically significant conclusion, relevant for our understanding of galaxy evolution. With that in mind, techniques such as stacking are used, to allow retrieval of statistical observations, while drastically reducing the need for observing time.

Stacking is a method first developed for optical data (Cady and Bates, 1980) that allows a statistical improvement of the SNR through averaging many individuals from an, à priori, similar population together. If the noise is Gaussian, and it should be in the first approximation, averaging N stamps of pixels together will improve the SNR by a factor $\sqrt{N}$, and hence lead to reveal patterns that were invisible before. Because stacking works through averaging, only patterns common to all (or at least most) sources will be properly enhanced, the other properties ending up being smeared out. This is the reason why a good à priori knowledge of the stacked sample is needed, to be sure that stacked sources share common properties.

Thus, the usage of statistical tools, to probe both the initial populations (if possible) and, mainly, the properties of the resulting stack, are essential. Let us consider that we want to measure the average size of the adult population of a town for example. If we simply average the size of every citizen together, kids will also also be included in our sample, driving down the average size. By randomly resampling the original sample into smaller size samples, a high number of times, we would eventually realize that the entire population is not homogeneous, composed of two distinct populations, of different average sizes. In this chapter I am going to discuss the details of the stacking algorithm I developed, as well as the data

analysis/statistical tools included in the code. Figure 4.1 shows an example of line stacking.

4.1 Main algorithm

The stacking tool I have developed, called Line-Stacker, is based on Stacker (Lindroos et al., 2015, 2016). It is an ensemble of CASA tasks and enables stacking of interferometric data. Unlike Stacker it allows stacking not only of continuum data but of spectral cubes. The goal is to stack together emission (or absorption) lines. To do so it simply requires the redshift of the targets, the rest frequency of the line to stack, and the spatial position of the targets. A 3D stamp (of user defined size), centered on each source both in space and in the spectral dimension (using the redshift), is extracted from the data and buffered, to facilitate access. Every stamp are then averaged together, pixel to pixel, spectral channel to spectral channel.

3D pixel averaging can be operated either through mean, median or weighted mean. Some weighting methods are embedded in Line-Stacker, although weights can also be specified by the user. Included weighting schemes are:

- $w_i = \frac{1}{\sigma_i^2}$ where w_i is the weight of source i and σ_i the standard deviation on the cube associated to source i. It is the most commonly used weighting methods, weighting sources inversely proportionally to the squared noise on the cube. Implying that all targets on the same cube will have the same weight, and that weights will be the same on all spectral channel (see Paper II).
- $w_{i,j} = \frac{1}{\sigma_{i,j}^2}$ where $w_{i,j}$ is the weight of target source i at spectral channel j, and $\sigma_{i,j}$ is the standard deviation of the cube associated to source i at spectral channel j. This method, similar to Fruchter and Hook (2002); Bischetti et al. (2018), allows to define individual weights for each spectral channel. This method can be especially useful if stacking data with large bandwidth, where the noise characteristics may be very different from one end of the bandwidth to the other.
- $w_i = \frac{1}{A_i}$ where A_i is the amplitude of the line associated to source i. This method can only be used if the lines are visible pre-stacking, and allows for an homogenization of the stack product (see Paper II).

A particular issue arising from stacking spectral lines, and not solely continuum, is the necessity for a specific treatment when trying to stack spectral bins outside of the observed spectral window. This can happen if the user requested large spectral stamps and/or if the observations are not centered on the line targeted for stacking. In such a case the algorithm has been build to not include these sources when stacking such channels. Because of this, less sources will be stacked in the outer channels, thus resulting in a higher noise level far from the spectral center. Another method, used for example is Murray et al. (2014), is to fill the empty channels with zeros and still add them to the stack. While the method is technically simpler, it leads to biasing, since zeros will be added to the stack, thus artificially reducing the stack values in these channels. To allow the user to have a good interpretation of their stack the algorithm returns the number of sources stacked in

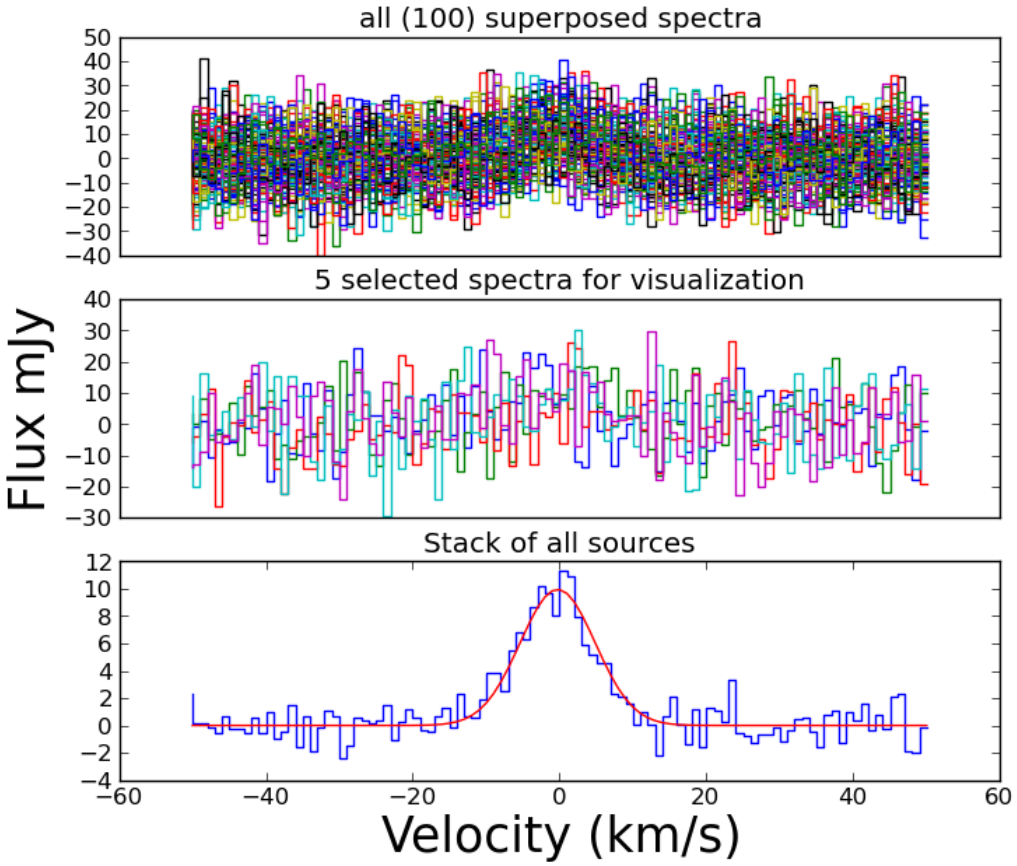

Figure 4.1: 1D stacking example of 100 spectra.

each spectral channel. The stack output is a stacked cube, leaving the user free to extract spectra in any desired fashion.

For completion, a 1D version of Line-Stacker is also included. The so called 1D-Stacker functions similarly to Line-Stacker, but stacks directly spectra and not cubes, and thus does not require spatial positions of the source to operate. The 1D-Stacker can be used on all kind of spectral-data extracted beforehand. It features the same tools as 3D Line-Stacker. 1D-Stacker is useful when users wish to extract spectra from the cubes before stacking. This can happen if sources have been observed with different telescopes or in different configuration, resulting for example in different primary beam. Similarly, if the sources are known to be extended, and of different size, it may be relevant to have a customized spectra extraction for each source (i.e. from a different region size) before stacking.

4.2 Embedded tools

To further the usefulness and capacities of Line-Stacker, I have developed a series of computing tools, embedded in the program and that can be used, either pre-stacking (to improve the knowledge on the studied data) or post-stacking, to get a better handling of the statistics, and to better understand the product of stacking.

One should bear in mind that, stacking being a statistical method, its product is not fully straightforward to analyze. These tools aim at providing the user with ways to perform and analyze stacking in a controlled and meaningful way.

4.2.1 Evaluating relevance of stack

Stack product should always be compared, not to the general noise in sources pre-stacking but to a "noise-stack": stacking where the stacking positions are fully chosen from random, "empty" (i.e. noise only), positions. To generate this "noise-stack" a set of positions on the images are randomly chosen (as many random positions as there are original target sources) and then stacked. This process is coupled to Monte Carlo methods to avoid peculiar noise regions, each time positions are randomized anywhere on the map, excluding a given region around the target sources (to avoid contamination). These stacks from random, source free, positions are then compared to the original stack, allowing to see whether the staking result could be reproduced by stacking solely random noise.

4.2.2 Bootstraping and subsampling

Bootstrapping and subsampling are statistical methods aiming at studying the distribution of the target sources' parameters, through randomly resampling the original set of sources. Coupled to Monte Carlo methods these processes are operated a high number of times to explore a representative portion of the total number of possible resamples.

Bootstrapping acts through randomly resampling with replacement, leading to a resampled population the same size as the original sample. When used through Line-Stacker, all subsequent resamples are stacked, and the corresponding stack result is saved. The distribution of stack results is then analyzed and compared to the original stack. The distribution should be close to Gaussian, centered on the original stack result – however, a bigger negative tail is expected since noise reduction is not optimal when a given source is present more than once in the stack. An inhomogeneous original sample distribution (with some outliers among the population for example) would lead to a possible strong deviation from Gaussianity and would hence be diagnosed as such by a bootstrapping analysis.

Subsampling acts through creation of a new, smaller, sample, randomly selected from the original sources. The number of elements N_{sub} in the new subsample can be fixed or randomized for each iteration of the Monte Carlo process, with $N_{min} < N_{sub} < N_{max}$ where $N_{min} > 0$ and $N_{max} < N$ – with N the number of sources in the original sample. N_{min} and N_{max} being input by the user. It should be noted that if N_{sub} is small, the noise reduction effect of stacking will be drastically reduced (because of the low number of sources in the stack); additionally, spanning all possible configurations will be a lengthy process, as there are

$$\binom{N}{N_{sub}} = \frac{N!}{N_{sub}!\,(N - N_{sub})!}$$

possible subsamples of size N_{sub}.

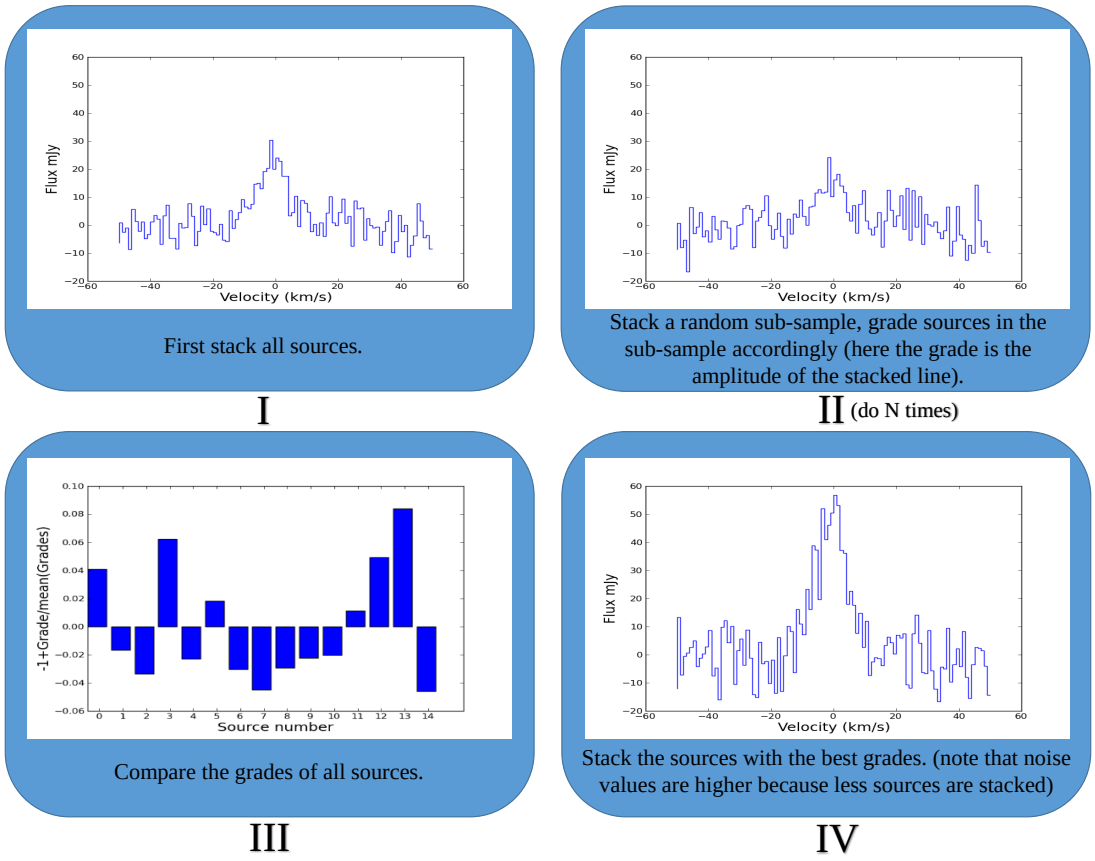

Figure 4.2: Sub-sampling: block-diagram example

Subsampling can, for example, be used if one expects that some sources should not be included in the stack, due to physical considerations (such, for example, as angular orientation in the case of QSO, see Paper II). To identify such sources subsampling should be paired with a grading function, attributing a common grade to sources in the tested subsample (see Figure 4.2). The exact grading function has to be user input, because dependent on the tested property. For example, in Paper II, the grading function would grade a subsample proportionally to the presence of spectral outflow signature. A pre-existing grading function is already embedded in Line-Stacker, grading the subsample proportionally to the corresponding stack's amplitude. Such method could allow to detect sources that are responsible for most of the emission, or that have a high probability to exhibit no – or much lower than average – emission.

4.2.3 Spectral rebinning

When trying to recover information about the line profile through stacking, one should be aware that stacking lines of different sizes or shapes will lead to a biased result. Since spectral stacking is performed spectral bin to spectral bin, stacking Gaussian shaped lines with a different width (in bins) will result in a non-Gaussian stacked profile, with wings (i.e. some additional flux in the outer channels, see Paper I). More generally, even if all sources exhibit lines with the same arbitrary shape

(Gaussian, Lorentzian, double peak Gaussian etc.), if they do not span the same amount of spectral bins, the shape information will be lost – or at least diluted – in the resulting stack. To prevent this problem a solution exists, as long as the lines are visible before stacking. It consists in rebinning all spectra so that all lines span the same amount of bins. It should be however noted that the bin size information is lost through rebinning: while before rebinning all spectral bins should have a definite physical size (i.e. in $\mathrm{km\,s^{-1}}$ or Hz), once rebinned all spectra show a different bin size. As such, deriving the size of the spectral channels, in the stack of rebinned spectra, is not straightforward.

It should be noted that, since there is no reason to expect all lines to have the same width naturally, it will be basically impossible to retrieve, with confidence, spectral shapes from sources invisible before stacking.

CHAPTER 5

RESULTS OF PAPERS

5.1 Paper I

5.1.1 Description of Paper I

Paper I aims at fully describing and testing Line-Stacker. To do so I simulated a number of data sets – data cubes as well as 1D data – to assess the tool performances in different situations. Most simulations are performed using CASA task SIMALMA: a task performing full ALMA observation simulation, taking a user custom sky input as the observable, delivering the set of visibilities as an output. Visibilities are then transformed into an image using the CLEAN algorithm (first developed in Högbom, 1974). All the stacks consist of 30 sources – yielding a noise reduction of $\sim \sqrt{30} \sim 5.5$. Each source consists solely of an emission line and some noise. The different simulated data sets are build to be increasingly realistic. The first sets being very simple, building slowly into more specific test cases that can be expected from real observations. Among other, the effects coming from: bright foreground sources, extended target sources or using a different interferometer (VLA) have been tested. To complete our study, four 1-dimension data sets have been simulated. To test the performances of the 1D-Stacker, but mainly to study cases with more complex spectral configuration. A special attention has been given to the study of redshift uncertainties.

5.1.2 Results of Paper I

For a summary of the results, see Table 3, 4, 5 and 6 in Paper I. Reconstruction rates of the line amplitude are very satisfying, above, or close, to 90% for every set; even the most complicated ones being properly reconstructed. Reconstruction keeps similar values when the amplitude of the line is set to noise level, showing the efficiency of stacking regarding SNR improvement. Reconstruction of linewidth[1], as well as integrated flux show similar results. As mentioned previously, when all

[1]I will be referring to the Full Width Half Maximum (FWHM) of the line when referring to the width, or linewidth

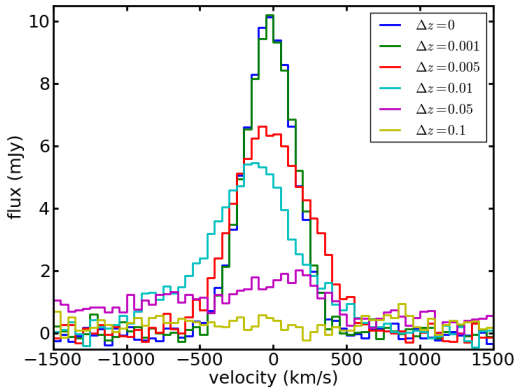

Figure 5.1: Stack spectrum of 30 sources of width 400 km s^{-1}, for different redshift uncertainties. $\Delta z = 0.01$ already shows a $\sim$ 50% reconstruction, an rapidly dropping.

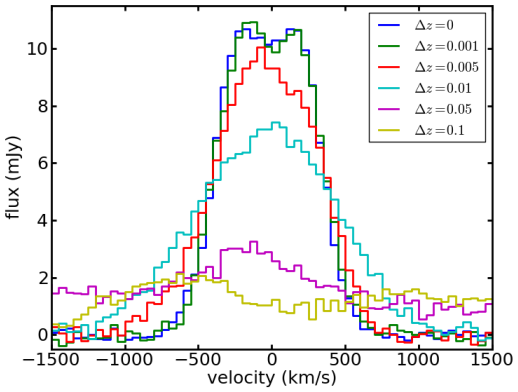

Figure 5.2: Stack spectrum of 30 sources of with double peak profile for different redshift uncertainties (both peaks are Gaussian, with a width of 400 km s^{-1}, and a distance of 400 km s^{-1} between the two peaks). An uncertainty higher than 0.001 already dilutes the two peaks, showing that similar profiles will be extremely hard to reconstruct through stacking.

lines have different width the resulting stacked line will lose its Gaussian shape. The amplitude will hence be slightly under-estimated by Gaussian fitting. While it does not have a huge impact on the results one should keep in mind this problem, inherent to spectral stacking.

Through stacking 1D simulated data sets, I quantified the effect of redshift uncertainties on spectral stacking. I showed that line reconstruction would be very inefficient for redshift uncertainties above 0.01. Furthermore trying to reconstruct line profiles is quasi-impossible if the redshift precision is not perfect. See Figures 5.1 and 5.2.

5.2 Paper II

5.2.1 Description of Paper II

Paper II is our first application of LINE-STACKER on real data. In this project we stacked a sample of 25 quasars at redshifts $z \sim 6$ detected in [CII], to search for a high velocity outflow component. As the main line of the host galaxy is clearly detected, and the redshift uncertainty is very low ($\Delta z < 0.01$), stacking can be performed accurately: with all the lines properly centered. Furthermore the good identification of individual line width allows for spectral rebinning of the individual spectra, avoiding issues that would arise from stacking lines with different width. Indeed, we showed that stacking lines with different width, introduces artificial wings signature into the stack, making the analysis of the spectral profile biased toward

finding outflows, if not rebinned beforehand. The goal of the project is to try and identify, through stacking, an outflow component, characterized by a second, broader and fainter, Gaussian component under the main line (see for example Sulentic et al., 2014; Decarli et al., 2018). As stated in section 2.4 outflow observation at high-redshift are needed to complete our understanding of the impact of AGN feedback on galaxy evolution.

Because it is expected that, even if all sources were to have outflows, they would not all be visible due to orientation effects, we used a subsampling method to identify sources presenting a clearer outflow component when stacked. We performed two stacking techniques:

- Firstly, spectra have been extracted, individually from each source, from the two-sigma region in moment-0 maps. All spectra were stacked together using 1D stacking. While this method is simpler and allows for a good and physical way to extract spectra, it is also biased: because the spectra are extracted before stacking, the potential outflow components are not individually detected, and it is not clear that they will span the same region as the main line. By restricting the extracting region to two-sigma we may be actually missing the regions where the outflow is, if the emission is extended for example. On the contrary, if the outflow emission is very compact, taking a too large region will lower the outflow signal (through summing pixels with no outflow component with pixels that do contain some).
- The other method consists of stacking the cubes, and extracting a spectrum afterwards, from the stacked cube. This allows us to examine the spatial extent and characteristics of the stacked line, but also has certain caveats. Since sources are stacked pixel to pixel, if the emission is more extended in some sources than in others, stacking could dilute the outflow signal. Furthermore, finding the good region from which to extract the spectrum is not straightforward.

However, both method showed similar results. Additionally, three weighting schemes have been used. The first being simply to use no weighting at all: Since that we do not know if there is a relation between main component and outflow component, it may be arbitrary to choose a peculiar weighting scheme, based on the main component characteristics. However, if one thinks that the outflow amplitude is proportional to the main line amplitude, then using a weighting inversely proportional to the amplitude of the line would allow all outflows to carry the same weight, correcting for their brightness. The last set of weights used is inversely proportional to the noise in the associated cube, allowing to give higher weights to sources presenting lower noise values.

5.2.2 Results of Paper II

Through subsampling we identified a sub-sample of 11 sources contributing to the majority of the broad component emission. We named this subsample "max sub-sample". Similarly we formed a sub-sample with the sources not included in the max sub-sample: the "min sub-sample". The stack of the max sub-sample shows a tentative detection of a broad component, with FWHM $= 1110 \pm 203\,\mathrm{km\,s^{-1}}$

and $S_{\rm peak} = 2.03 \pm 0.61\,{\rm mJy}$, which is indicative of a [CII] outflow. Furthermore, when stacking the min sub-sample we find no deviation from simple Gaussianity, indicating coherence in our subsampling scheme.

To make sure that the obtained results are neither purely random nor driven by one, brighter, source, we performed mock sample tests and additional analysis of our sample: to verify that one source was not single-handedly responsible for most of the outflow emission we performed the stack of the subsample, after removing one of its source. We repeated this process for each source in the subsample. The resulting stacks showed not strong deviation from the original max sub-sample stack, we concluded that the max sub-sample was rather homogeneous, in terms of wings emission. Additionally, we performed tests to make sure that our signal could not be reproduced by stacking random noise. Finally, to prove the efficiency of our methods we created mock data-sets containing outflows to determine their recovery rate. The outflow were generated with a width of three times the main component's, and an amplitude five times weaker than the main component's. By stacking we attained a recovery rate of the second component of 98.52% at $3\,\sigma$ and 31.72% at $5\,\sigma$, showing that our method should be able to recover outflow with similar properties, to a least $3\,\sigma$.

Our results are consistent with molecular outflows observations at low and high redshifts (e.g. Harrison et al., 2014; Cicone, 2015), both for the derived width and amplitude of the second component. While deeper, individual, observations would be needed to improve our understanding of outflows at $z \sim 6$, our study is a first step in quantifying the detectability of high-redshift outflows, and will be useful when planing individual observations. In addition, we showed the efficiency of subsampling, that could be combined with large surveys to identify sources more likely to present an outflow component.

My contribution to Paper II is that I developed the stacking tool (as described in Paper I), carried out the stacking analysis, including the subsampling, and performed the mock sample tests mentioned above. Additionally I participated in the data reduction.

CHAPTER 6

OUTLOOK

With LINE-STACKER now fully operational future perspectives come to mind. I will first discuss expected extensions of the tool, followed by science topics to which LINE-STACKER could be applied, or the questions it could help answer to.

6.1 Methodology

6.1.1 Stacking in the *uv*-plane

The first obvious extension of LINE-STACKER is to make it usable to stack directly visibilities. The original STACKER had been developed with a focus on *uv* stacking, and it has been showed that it allows:

- Better treatment of problematic baselines, through directly removing them while stacking.
- Better estimate of the physical extent of stacked sources.
- Better noise treatment (noise on data points is fully independent in the *uv*-plane).
- Better removal of artifacts from bright sources.
- Better treatment of data sets with different *uv*-coverage (such a case would results in different resolutions for each image: they would hence need to be converted to the same resolution, resulting in data loss).

It can be expected that conclusions similar to Lindroos et al. (2015) will be drawn from doing spectral *uv*-stacking. Indeed there is no drastic difference between spectral stacking and continuum stacking, and the outcome from both spectral stacking in the image-plane and continuum stacking in the *uv*-plane should combine. However, while rather better in quite a few situations, *uv*-stacking also happens to be computationally more expensive. While stacking once is not sufficiently slow to be a problem, it could become an issue when using Monte Carlo processes to perform statistical analysis of the stack.

6.1.2 Improving redshifts through line stacking

Another method, that as been thought of and that will be implemented into LINE-STACKER, once built and tested, is the possibility to improve individual redshifts from the stacked sources. As shown in Paper I, an imprecision on the redshift implies a broadening and an amplitude diminution of the line. By using an algorithm allowing to sample the probability distribution (such as Markov Chains Monte Carlo) one might be able to retrieve the redshifts maximizing the stacked line's amplitude, i.e. the true redshifts of the lines. This works the following way: The algorithm starts from the originally estimated redshifts of each line, and computes the corresponding stacked line. The redshifts are then slightly changed and the new corresponding stacked line is computed. If the amplitude of the new stacked line is higher than the amplitude of the original one it means that the new set of redshifts is closer to the true redshifts. This process is operated a high number of time, randomly drawing new redshifts. Ultimately, if the algorithm is properly built and if convergence is possible, the algorithm could be able to fully maximize the stacked line and hence find the redshifts closest to the true redshifts.

6.2 Scientific outlook with Line-Stacker

6.2.1 Gas mass fraction across redshifts

Understanding star formation is a very important step to complete our description of galaxy evolution. The link between star formation and atomic/molecular gas is essential, but yet poorly understood (e.g. Lagos et al., 2012). Models and analytical descriptions have been developed, trying to clarify the relation between star formation and gas mass fraction (e.g. Lagos et al., 2012; Popping et al., 2014; Lagos et al., 2014). While accurate measurements of HI in local galaxies (Zwaan et al., 2005; Martin et al., 2010) have been performed, there seems to be no evolution of the global HI mass density up to $z \sim 5$ (e.g. Péroux et al., 2003; Noterdaeme et al., 2009). Meanwhile the global star formation rate density is known to peak around $z \sim$ 2-3, before decreasing at higher redshift. Such a misalignment would imply that HI is not the direct fuel of star formation. A good candidate then, would be H_2 (Lagos et al., 2014), usually traced by the CO molecule. However, there is only a limited number of CO observations, and mainly at low redshift (Keres et al., 2003) or focused on bright galaxies (e.g. review by Carilli and Walter, 2013; Tacconi et al., 2013), preventing a good complete description of its evolution. Using LINE-STACKER we could perform accurate measurements of the H_2 density in faint high-redshift galaxies, allowing to build up a proper correlation between the evolution the H_2 content and star formation rate density across redshifts.

6.2.2 How passive are massive passive galaxies?

Passive, low star formation rates galaxies have been observed in a large redshift range (see Daddi et al., 2005; Hopkins et al., 2008; Merlin et al., 2018). As an example, Kriek et al. (2006) show that ∼50% of the galaxies in their sample at $z \sim 2.3$

do not show any emission line. However, their observations were performed in the near-infrared, and such sources should probably be studied with sensitive mm observations to search for molecular gas and dust emission. Furthermore, using stacking would have allowed, if not a detection, to push down the upper limit significantly (by a factor $\sqrt{20} \sim 4.4$). As shown in Simpson et al. (2017), properly classifying a galaxy as quiescent is challenging, especially at high redshift, and requires multi-wavelength high-resolution observations. Furthermore, Spilker et al. (2018) show that some amount of molecular gas can be expected even from galaxies way below the main sequence of star forming galaxies, successfully detecting gas fraction $\lesssim 0.1$ in half of their sample. LINE-STACKER would be perfectly suited to perform this kind of analysis, and could allow to redefine the status of passive galaxies, by properly quantifying their gas fraction.

6.2.3 Gas-to-dust ratio in high-redshift galaxies & subsampling

The gas-to-dust ratio traces the evolutionary stage of a galaxy and is linked to galactic metallicity (Issa et al., 1990; Rémy-Ruyer et al., 2014). Cortese et al. (2016) have computed both the atomic and molecular gas-to-dust ratio of a large sample of local galaxies, trying to show the impact of the environment on the said ratios. Using LINE-STACKER on large samples one could characterise both the atomic and molecular gas-to-dust ratios in high-redshift galaxies, leading to a better description of metallicity with redshift. Furthermore, if applied to really large samples (e.g. Laigle et al., 2016) the use of subsampling could allow to divide the entire data-set in smaller chunks presenting different ratio values. Allowing either to draw up the evolution of the ratio with redshift, or linking specific gas-to-dust ratios to specific galaxy group.

6.2.4 Outflows in QSO at low/intermediate redshifts

In Paper II we stacked a sample of $z \sim 6$ QSO, searching for molecular [CII] outflows. While similar molecular outflows have been detected at low to intermediate redshifts (e.g. Aalto et al., 2012; Rupke and Veilleux, 2013; Maiolino et al., 2012; Cicone et al., 2014), there are only a handful, individual detection. Meanwhile, low redshift detections have enabled the study of outflow properties as a function of other galaxy properties (e.g. Cicone et al., 2014). Now that the analysis we developed in Paper II is well characterised and proved its efficiency, we could, using big data sets, try to characterize the evolution of molecular outflow properties with redshift. Linking outflow characteristics to galactic properties, specifically star formation.

BIBLIOGRAPHY

Aalto, S., Muller, S., Sakamoto, K., Gallagher, J. S., Martín, S., and Costagliola, F. (2012). Winds of change - a molecular outflow in NGC 1377?. The anatomy of an extreme FIR-excess galaxy. , 546:A68.

Alexander, D. M. and Hickox, R. C. (2012). What drives the growth of black holes? *New Astronomy Reviews*, 56:93–121.

Baldry, I. K. (2008). Hubble's galaxy nomenclature. *Astronomy & Geophysics*, 49(5):5–25.

Barnes, J. E. and Hernquist, L. (1996). Transformations of Galaxies. II. Gasdynamics in Merging Disk Galaxies. , 471:115.

Bertone, S. and Conselice, C. J. (2009). A comparison of galaxy merger history observations and predictions from semi-analytic models. , 396:2345–2358.

Bischetti, M., Maiolino, R., Fiore, S. C. F., Piconcelli, E., and Fluetsch, A. (2018). Widespread QSO-driven outflows in the early Universe. *ArXiv e-prints*.

Cady, F. M. and Bates, R. H. T. (1980). Speckle processing gives diffraction-limited true images from severely aberrated instruments. *Optics Letters*, 5:438–440.

Carilli, C. L. and Walter, F. (2013). Cool Gas in High-Redshift Galaxies. *Annual Review of Astronomy and Astrophysics*, 51:105–161.

Carrasco, E. R., Gomez, P. L., Verdugo, T., Lee, H., Diaz, R., Bergmann, M., Turner, J. E. H., Miller, B. W., and West, M. J. (2010). Strong Gravitational Lensing by the Super-massive cD Galaxy in Abell 3827. , 715:L160–L164.

Cicone, C. (2015). Powerful quasar feedback in local and very distant galaxies. In *IAU General Assembly*, volume 29, page 2245440.

Cicone, C., Maiolino, R., Sturm, E., Graciá-Carpio, J., Feruglio, C., Neri, R., Aalto, S., Davies, R., Fiore, F., Fischer, J., García-Burillo, S., González-Alfonso, E., Hailey-Dunsheath, S., Piconcelli, E., and Veilleux, S. (2014). Massive molecular outflows and evidence for AGN feedback from CO observations. , 562:A21.

Circosta, C., Mainieri, V., Padovani, P., Lanzuisi, G., Salvato, M., Harrison, C. M., Kakkad, D., Puglisi, A., Vietri, G., Zamorani, G., Cicone, C., Husemann, B., Vignali, C., Balmaverde, B., Bischetti, M., Bongiorno, A., Brusa, M., Carniani, S., Civano, F., Comastri, A., Cresci, G., Feruglio, C., Fiore, F., Fotopoulou, S., Karim, A., Lamastra, A., Magnelli, B., Mannucci, F., Marconi, A., Merloni, A., Netzer, H., Perna, M., Piconcelli, E., Rodighiero, G., Schinnerer, E., Schramm, M., Schulze, A., Silverman, J., and Zappacosta, L. (2018). SUPER. I. Toward an unbiased study of ionized outflows in z 2 active galactic nuclei: survey overview and sample characterization. , 620:A82.

Clark, P. C., Glover, S. C. O., Ragan, S. E., and Duarte-Cabral, A. (2018). Tracing the formation of molecular clouds via [CII], [CI] and CO emission. *arXiv e-prints*, page arXiv:1809.00489.

Coc, A. and Vangioni, E. (2017). Primordial nucleosynthesis. *International Journal of Modern Physics E*, 26:1741002.

Cortese, L., Bekki, K., Boselli, A., Catinella, B., Ciesla, L., Hughes, T. M., Baes, M., Bendo, G. J., Boquien, M., de Looze, I., Smith, M. W. L., Spinoglio, L., and Viaene, S. (2016). The selective effect of environment on the atomic and molecular gas-to-dust ratio of nearby galaxies in the Herschel Reference Survey. , 459:3574–3584.

Costagliola, F., Sakamoto, K., Muller, S., Martín, S., Aalto, S., Harada, N., van der Werf, P., Viti, S., Garcia-Burillo, S., and Spaans, M. (2015). Exploring the molecular chemistry and excitation in obscured luminous infrared galaxies. An ALMA mm-wave spectral scan of NGC 4418. , 582:A91.

Daddi, E., Cimatti, A., and Renzini, A. (2000). Eros and the formation epoch of field ellipticals. *arXiv preprint astro-ph/0010093*.

Daddi, E., Cimatti, A., Renzini, A., Fontana, A., Mignoli, M., Pozzetti, L., Tozzi, P., and Zamorani, G. (2004). A new photometric technique for the joint selection of star-forming and passive galaxies at 1.4 z 2.5. *The Astrophysical Journal*, 617(2):746.

Daddi, E., Renzini, A., Pirzkal, N., Cimatti, A., Malhotra, S., Stiavelli, M., Xu, C., Pasquali, A., Rhoads, J. E., Brusa, M., di Serego Alighieri, S., Ferguson, H. C., Koekemoer, A. M., Moustakas, L. A., Panagia, N., and Windhorst, R. A. (2005). Passively Evolving Early-Type Galaxies at 1.4 <~z <~2.5 in the Hubble Ultra Deep Field. , 626:680–697.

Decarli, R., Walter, F., Venemans, B. P., Bañados, E., Bertoldi, F., Carilli, C., Fan, X., Farina, E. P., Mazzucchelli, C., Riechers, D., Rix, H.-W., Strauss, M. A., Wang, R., and Yang, Y. (2018). An ALMA [C II] Survey of 27 Quasars at z 5.94. , 854:97.

Dekel, A., Birnboim, Y., Engel, G., Freundlich, J., Goerdt, T., Mumcuoglu, M., Neistein, E., Pichon, C., Teyssier, R., and Zinger, E. (2009). Cold streams in early massive hot haloes as the main mode of galaxy formation. *Nature*, 457(7228):451.

Dey, A., Soifer, B., Desai, V., Brand, K., Le Floc'h, E., Brown, M. J., Jannuzi, B. T., Armus, L., Bussmann, S., Brodwin, M., et al. (2008). A significant population of very luminous dust-obscured galaxies at redshift z˜ 2. *The Astrophysical Journal*, 677(2):943.

Di Matteo, T., Springel, V., and Hernquist, L. (2005). Energy input from quasars regulates the growth and activity of black holes and their host galaxies. , 433:604–607.

Dressler, A. and Richstone, D. O. (1988). Stellar Dynamics in the Nuclei of M31 and M32: Evidence for Massive Black Holes. , 324:701.

Fabian, A. C. (2012). Observational Evidence of Active Galactic Nuclei Feedback. *Annual Review of Astronomy and Astrophysics*, 50:455–489.

Franx, M., Labbe, I., Rudnick, G., van Dokkum, P. G., Daddi, E., Schreiber, N. M. F., Moorwood, A., Rix, H.-W., Röttgering, H., van de Wel, A., et al. (2003). A significant population of red, near-infrared-selected high-redshift galaxies. *The Astrophysical Journal Letters*, 587(2):L79.

Fruchter, A. S. and Hook, R. N. (2002). Drizzle: A Method for the Linear Reconstruction of Undersampled Images. *Publications of the Astronomical Society of the Pacific*, 114:144–152.

Häring, N. and Rix, H.-W. (2004). On the Black Hole Mass-Bulge Mass Relation. , 604:L89–L92.

Harms, R. J., Ford, H. C., Tsvetanov, Z. I., Hartig, G. F., Dressel, L. L., Kriss, G. A., Bohlin, R., Davidsen, A. F., Margon, B., and Kochhar, A. K. (1994). HST FOS Spectroscopy of M87: Evidence for a Disk of Ionized Gas around a Massive Black Hole. , 435:L35.

Harrison, C. M., Alexander, D. M., Mullaney, J. R., and Swinbank, A. M. (2014). Kiloparsec-scale outflows are prevalent among luminous AGN: outflows and feedback in the context of the overall AGN population. , 441:3306–3347.

Harrison, C. M., Costa, T., Tadhunter, C. N., Flütsch, A., Kakkad, D., Perna, M., and Vietri, G. (2018). AGN outflows and feedback twenty years on. *Nature Astronomy*, 2:198–205.

Henkel, C., Mühle, S., Bendo, G., Józsa, G. I. G., Gong, Y., Viti, S., Aalto, S., Combes, F., García-Burillo, S., Hunt, L. K., Mangum, J., Martín, S., Muller, S., Ott, J., van der Werf, P., Malawi, A. A., Ismail, H., Alkhuja, E., Asiri, H. M., Aladro, R., Alves, F., Ao, Y., Baan, W. A., Costagliola, F., Fuller, G., Greene, J., Impellizzeri, C. M. V., Kamali, F., Klessen, R. S., Mauersberger, R., Tang, X. D., Tristram, K., Wang, M., and Zhang, J. S. (2018). Molecular line emission in NGC 4945, imaged with ALMA. , 615:A155.

Högbom, J. A. (1974). Aperture Synthesis with a Non-Regular Distribution of Interferometer Baselines. , 15:417.

Hopkins, P. F., Cox, T. J., Kereš, D., and Hernquist, L. (2007). Preprint typeset using latex style emulateapj v. 10/09/06 a cosmological framework for the co-evolution of quasars, supermassive black holes, and elliptical galaxies: Ii. formation of red ellipticals.

Hopkins, P. F., Cox, T. J., Kereš, D., and Hernquist, L. (2008). A Cosmological Framework for the Co-Evolution of Quasars, Supermassive Black Holes, and Elliptical Galaxies. II. Formation of Red Ellipticals. *The Astrophysical Journal Supplement Series*, 175:390–422.

Hopkins, P. F., Hernquist, L., Cox, T. J., Di Matteo, T., Robertson, B., and Springel, V. (2006). A unified, merger-driven model of the origin of starbursts, quasars, the cosmic x-ray background, supermassive black holes, and galaxy spheroids. *The Astrophysical Journal Supplement Series*, 163(1):1.

Issa, M. R., MacLaren, I., and Wolfendale, A. W. (1990). Dust-to-gas ratio and metallicity variations in nearby galaxies. , 236:237.

Katz, N., Keres, D., Dave, R., and Weinberg, D. H. (2003). How Do Galaxies Get Their Gas? In Rosenberg, J. L. and Putman, M. E., editors, *The IGM/Galaxy Connection. The Distribution of Baryons at z=0*, volume 281 of *Astrophysics and Space Science Library*, page 185.

Kauffmann, G., Heckman, T. M., Tremonti, C., Brinchmann, J., Charlot, S., White, S. D. M., Ridgway, S. E., Brinkmann, J., Fukugita, M., Hall, P. B., Ivezić, Ž., Richards, G. T., and Schneider, D. P. (2003). The host galaxies of active galactic nuclei. , 346:1055–1077.

Keres, D., Yun, M. S., and Young, J. S. (2003). CO Luminosity Functions for Far-Infrared- and B-Band-selected Galaxies and the First Estimate for Ω_{HI}+H_2. , 582:659–667.

Kereš, D., Katz, N., Weinberg, D. H., and Davé, R. (2005). How do galaxies get their gas? , 363:2–28.

Kirby, E. N., Boylan-Kolchin, M., Cohen, J. G., Geha, M., Bullock, J. S., and Kaplinghat, M. (2013). Segue 2: The Least Massive Galaxy. , 770:16.

Knudsen, K. K., Watson, D., Frayer, D., Christensen, L., Gallazzi, A., Michałowski, M. J., Richard, J., and Zavala, J. (2017). A merger in the dusty, z = 7.5 galaxy A1689-zD1? , 466:138–146.

Kriek, M., van Dokkum, P. G., Franx, M., Quadri, R., Gawiser, E., Herrera, D., Illingworth, G. D., Labbé, I., Lira, P., Marchesini, D., Rix, H.-W., Rudnick, G., Taylor, E. N., Toft, S., Urry, C. M., and Wuyts, S. (2006). Spectroscopic Identification of Massive Galaxies at z ˜ 2.3 with Strongly Suppressed Star Formation. , 649:L71–L74.

Lagache, G., Cousin, M., and Chatzikos, M. (2018). The [CII] 158 μm line emission in high-redshift galaxies. , 609:A130.

Lagos, C. D. P., Baugh, C. M., Zwaan, M. A., Lacey, C. G., Gonzalez-Perez, V.,

Power, C., Swinbank, A. M., and van Kampen, E. (2014). Which galaxies dominate the neutral gas content of the Universe? , 440:920–941.

Lagos, C. d. P., Bayet, E., Baugh, C. M., Lacey, C. G., Bell, T. A., Fanidakis, N., and Geach, J. E. (2012). Predictions for the CO emission of galaxies from a coupled simulation of galaxy formation and photon-dominated regions. , 426:2142–2165.

Laigle, C., McCracken, H. J., Ilbert, O., Hsieh, B. C., Davidzon, I., Capak, P., Hasinger, G., Silverman, J. D., Pichon, C., Coupon, J., Aussel, H., Le Borgne, D., Caputi, K., Cassata, P., Chang, Y. Y., Civano, F., Dunlop, J., Fynbo, J., Kartaltepe, J. S., Koekemoer, A., Le Fèvre, O., Le Floc'h, E., Leauthaud, A., Lilly, S., Lin, L., Marchesi, S., Milvang- Jensen, B., Salvato, M., Sanders, D. B., Scoville, N., Smolcic, V., Stockmann, M., Taniguchi, Y., Tasca, L., Toft, S., Vaccari, M., and Zabl, J. (2016). The COSMOS2015 Catalog: Exploring the 1 < z < 6 Universe with Half a Million Galaxies. *The Astrophysical Journal Supplement Series*, 224:24.

Le Fèvre, O., Sanjuan, C., Tasca, L., Vvds Team, Massiv Team, and Vuds Team (2013). The Galaxy Merger Rate History (GMRH) since z 3. In Sun, W. H., Xu, C. K., Scoville, N. Z., and Sanders, D. B., editors, *Galaxy Mergers in an Evolving Universe*, volume 477 of *Astronomical Society of the Pacific Conference Series*, page 133.

Lin, L., Patton, D. R., Koo, D. C., Casteels, K., Conselice, C. J., Faber, S., Lotz, J., Willmer, C. N., Hsieh, B., Chiueh, T., et al. (2008). The redshift evolution of wet, dry, and mixed galaxy mergers from close galaxy pairs in the deep2 galaxy redshift survey. *The Astrophysical Journal*, 681(1):232.

Lindroos, L., Knudsen, K. K., Fan, L., Conway, J., Coppin, K., Decarli, R., Drouart, G., Hodge, J. A., Karim, A., Simpson, J. M., and Wardlow, J. (2016). Estimating sizes of faint, distant galaxies in the submillimetre regime. , 462:1192–1202.

Lindroos, L., Knudsen, K. K., Vlemmings, W., Conway, J., and Martí-Vidal, I. (2015). Stacking of large interferometric data sets in the image- and uv-domain - a comparative study. , 446:3502–3515.

Lynden-Bell, D. (1969). Galactic Nuclei as Collapsed Old Quasars. , 223:690–694.

Maiolino, R., Gallerani, S., Neri, R., Cicone, C., Ferrara, A., Genzel, R., Lutz, D., Sturm, E., Tacconi, L. J., Walter, F., Feruglio, C., Fiore, F., and Piconcelli, E. (2012). Evidence of strong quasar feedback in the early Universe. , 425:L66–L70.

Marconi, A. and Hunt, L. K. (2003). The Relation between Black Hole Mass, Bulge Mass, and Near-Infrared Luminosity. , 589:L21–L24.

Martin, A. M., Papastergis, E., Giovanelli, R., Haynes, M. P., Springob, C. M., and Stierwalt, S. (2010). The Arecibo Legacy Fast ALFA Survey. X. The H I Mass Function and Ω_H I from the 40% ALFALFA Survey. , 723:1359–1374.

Martin, N. F., Ibata, R. A., Bellazzini, M., Irwin, M. J., Lewis, G. F., and Dehnen, W. (2004). A dwarf galaxy remnant in Canis Major: the fossil of an in-plane accretion on to the Milky Way. , 348:12–23.

Merlin, E., Fontana, A., Castellano, M., Santini, P., Torelli, M., Boutsia, K., Wang, T., Grazian, A., Pentericci, L., Schreiber, C., Ciesla, L., McLure, R., Derriere, S., Dunlop, J. S., and Elbaz, D. (2018). Chasing passive galaxies in the early Universe: a critical analysis in CANDELS GOODS-South. , 473:2098–2123.

Morganti, R., de Zeeuw, P. T., Oosterloo, T. A., McDermid, R. M., Krajnović, D., Cappellari, M., Kenn, F., Weijmans, A., and Sarzi, M. (2006). Neutral hydrogen in nearby elliptical and lenticular galaxies: the continuing formation of early-type galaxies. , 371:157–169.

Murray, C. E., Lindner, R. R., Stanimirović, S., Goss, W. M., Heiles, C., Dickey, J., Pingel, N. M., Lawrence, A., Jencson, J., Babler, B. L., and Hennebelle, P. (2014). Excitation Temperature of the Warm Neutral Medium as a New Probe of the Lyα Radiation Field. , 781:L41.

Naab, T., Johansson, P. H., and Ostriker, J. P. (2009). Minor Mergers and the Size Evolution of Elliptical Galaxies. , 699:L178–L182.

Naab, T. and Ostriker, J. P. (2017). Theoretical Challenges in Galaxy Formation. *Annual Review of Astronomy and Astrophysics*, 55:59–109.

Noterdaeme, P., Petitjean, P., Ledoux, C., and Srianand, R. (2009). Evolution of the cosmological mass density of neutral gas from Sloan Digital Sky Survey II - Data Release 7. , 505:1087–1098.

Okumura, T., Matsubara, T., Eisenstein, D. J., Kayo, I., Hikage, C., Szalay, A. S., and Schneider, D. P. (2008). Large-Scale Anisotropic Correlation Function of SDSS Luminous Red Galaxies. , 676:889–898.

Omont, A. (2007). Molecules in galaxies. *Reports on Progress in Physics*, 70:1099–1176.

Péroux, C., McMahon, R. G., Storrie-Lombardi, L. J., and Irwin, M. J. (2003). The evolution of Ω_{HI} and the epoch of formation of damped Lyman α absorbers. , 346:1103–1115.

Persic, M. and Salucci, P. (1992). The baryon content of the universe. , 258:14P–18P.

Pettini, M. and Pagel, B. E. J. (2004). [OIII]/[NII] as an abundance indicator at high redshift. , 348:L59–L63.

Planck Collaboration (2016). Planck 2015 results. I. Overview of products and scientific results. , 594:A1.

Popping, G., Somerville, R. S., and Trager, S. C. (2014). Evolution of the atomic and molecular gas content of galaxies. , 442:2398–2418.

Rees, M. J. (1984). Black Hole Models for Active Galactic Nuclei. *Annual Review of Astronomy and Astrophysics*, 22:471–506.

Rémy-Ruyer, A., Madden, S. C., Galliano, F., Galametz, M., Takeuchi, T. T., Asano, R. S., Zhukovska, S., Lebouteiller, V., Cormier, D., Jones, A., Bocchio, M., Baes, M., Bendo, G. J., Boquien, M., Boselli, A., DeLooze, I., Doublier-Pritchard,

V., Hughes, T., Karczewski, O. Ł., and Spinoglio, L. (2014). Gas-to-dust mass ratios in local galaxies over a 2 dex metallicity range. , 563:A31.

Rodriguez-Gomez, V., Genel, S., Vogelsberger, M., Sijacki, D., Pillepich, A., Sales, L. V., Torrey, P., Snyder, G., Nelson, D., Springel, V., Ma, C.-P., and Hernquist, L. (2015). The merger rate of galaxies in the Illustris simulation: a comparison with observations and semi-empirical models. , 449:49–64.

Rupke, D. S. N. and Veilleux, S. (2011). Integral Field Spectroscopy of Massive, Kiloparsec-scale Outflows in the Infrared-luminous QSO Mrk 231. , 729:L27.

Rupke, D. S. N. and Veilleux, S. (2013). Breaking the Obscuring Screen: A Resolved Molecular Outflow in a Buried QSO. , 775:L15.

Sanders, D. B. and Mirabel, I. F. (1996). Luminous Infrared Galaxies. *Annual Review of Astronomy and Astrophysics*, 34:749.

Sargent, W. L. W., Young, P. J., Boksenberg, A., Shortridge, K., Lynds, C. R., and Hartwick, F. D. A. (1978). Dynamical evidence for a central mass concentration in the galaxy M87. , 221:731–744.

Schaye, J., Crain, R. A., Bower, R. G., Furlong, M., Schaller, M., Theuns, T., Dalla Vecchia, C., Frenk, C. S., McCarthy, I. G., Helly, J. C., Jenkins, A., Rosas-Guevara, Y. M., White, S. D. M., Baes, M., Booth, C. M., Camps, P., Navarro, J. F., Qu, Y., Rahmati, A., Sawala, T., Thomas, P. A., and Trayford, J. (2015). The EAGLE project: simulating the evolution and assembly of galaxies and their environments. , 446:521–554.

Scoville, N., Aussel, H., Sheth, K., Scott, K. S., Sanders, D., Ivison, R., Pope, A., Capak, P., Vanden Bout, P., Manohar, S., Kartaltepe, J., Robertson, B., and Lilly, S. (2014). The Evolution of Interstellar Medium Mass Probed by Dust Emission: ALMA Observations at z = 0.3-2. , 783:84.

Simpson, J. M., Smail, I., Wang, W.-H., Riechers, D., Dunlop, J. S., Ao, Y., Bourne, N., Bunker, A., Chapman, S. C., Chen, C.-C., Dannerbauer, H., Geach, J. E., Goto, T., Harrison, C. M., Hwang, H. S., Ivison, R. J., Kodama, T., Lee, C. H., Lee, H. M., Lee, M., Lim, C. F., Michałowski, M. J., Rosario, D. J., Shim, H., Shu, X. W., Swinbank, A. M., Tee, W. L., Toba, Y., Valiante, E., Wang, J., and Zheng, X. Z. (2017). An Imperfectly Passive Nature: Bright Submillimeter Emission from Dust-obscured Star Formation in the z = 3.717 "Passive" System, ZF 20115. , 844:L10.

Smith, J. D. T., Croxall, K., Draine, B., De Looze, I., Sandstrom, K., Armus, L., Beirão, P., Bolatto, A., Boquien, M., Brandl, B., Crocker, A., Dale, D. A., Galametz, M., Groves, B., Helou, G., Herrera-Camus, R., Hunt, L., Kennicutt, R., Walter, F., and Wolfire, M. (2017). The Spatially Resolved [CII] Cooling Line Deficit in Galaxies. , 834:5.

Somerville, R. S., Hopkins, P. F., Cox, T. J., Robertson, B. E., and Hernquist, L. (2008). A semi-analytic model for the co-evolution of galaxies, black holes and active galactic nuclei. , 391:481–506.

Spilker, J., Bezanson, R., Barišić, I., Bell, E., Lagos, C. d. P., Maseda, M., Muzzin, A., Pacifici, C., Sobral, D., Straatman, C., van der Wel, A., van Dokkum, P., Weiner, B., Whitaker, K., Williams, C. C., and Wu, P.-F. (2018). Molecular Gas Contents and Scaling Relations for Massive, Passive Galaxies at Intermediate Redshifts from the LEGA-C Survey. , 860:103.

Springel, V., White, S. D., Jenkins, A., Frenk, C. S., Yoshida, N., Gao, L., Navarro, J., Thacker, R., Croton, D., Helly, J., et al. (2005). Simulations of the formation, evolution and clustering of galaxies and quasars. *nature*, 435(7042):629.

Steidel, C. C., Giavalisco, M., Pettini, M., Dickinson, M., and Adelberger, K. L. (1996). Spectroscopic confirmation of a population of normal star-forming galaxies at redshifts z> 3. *The Astrophysical Journal Letters*, 462(1):L17.

Stutzki, J., Graf, U. U., Haas, S., Honingh, C. E., Hottgenroth, D., Jacobs, K., Schieder, R., Simon, R., Staguhn, J., Winnewisser, G., Martin, R. N., Peters, W. L., and McMullin, J. P. (1997). Atomic Carbon in M82: Physical Conditions Derived from Simultaneous Observations of the [C I] Fine-Structure Submillimeter-Wave Transitions. , 477:L33–L36.

Sulentic, J., Marziani, P., Dultzin, D., D'Onofrio, M., and del Olmo, A. (2014). Fifty years of quasars: physical insights and potential for cosmology. In *Journal of Physics: Conference Series*, volume 565, page 012018. IOP Publishing.

Tacconi, L. J., Neri, R., Genzel, R., Combes, F., Bolatto, A., Cooper, M. C., Wuyts, S., Bournaud, F., Burkert, A., Comerford, J., Cox, P., Davis, M., Förster Schreiber, N. M., García-Burillo, S., Gracia-Carpio, J., Lutz, D., Naab, T., Newman, S., Omont, A., Saintonge, A., Shapiro Griffin, K., Shapley, A., Sternberg, A., and Weiner, B. (2013). Phibss: Molecular Gas Content and Scaling Relations in z ˜ 1-3 Massive, Main-sequence Star-forming Galaxies. , 768:74.

Tanabashi, M. et al. (2018). Review of particle physics. *Phys. Rev. D*, 98:030001.

Tielens, A. G. (2005). *The physics and chemistry of the interstellar medium*. Cambridge University Press.

van der Marel, R. P., Besla, G., Cox, T. J., Sohn, S. T., and Anderson, J. (2012). The M31 Velocity Vector. III. Future Milky Way M31-M33 Orbital Evolution, Merging, and Fate of the Sun. , 753:9.

Vogelsberger, M., Genel, S., Springel, V., Torrey, P., Sijacki, D., Xu, D., Snyder, G., Bird, S., Nelson, D., and Hernquist, L. (2014). Properties of galaxies reproduced by a hydrodynamic simulation. *Nature*, 509(7499):177.

Walter, F., Brinks, E., de Blok, W. J. G., Bigiel, F., Kennicutt, Robert C., J., Thornley, M. D., and Leroy, A. (2008). THINGS: The H I Nearby Galaxy Survey. , 136:2563–2647.

White, S. D. M. and Rees, M. J. (1978). Core condensation in heavy halos - A two-stage theory for galaxy formation and clustering. , 183:341–358.

Zwaan, M. A., Kuntschner, H., Pracy, M. B., and Couch, W. J. (2013). The cold gas content of post-starburst galaxies. , 432:492–499.

Zwaan, M. A., Meyer, M. J., Staveley-Smith, L., and Webster, R. L. (2005). The HIPASS catalogue: Ω_{HI} and environmental effects on the HI mass function of galaxies. , 359:L30–L34.

Paper I

LINE-STACKER: A spectral line stacking tool for interferometric data

J-B. Jolly, K. K. Knudsen, F. Stanley, J. Conway

Manuscript intended for Monthly Notices of the Royal Astronomical Society

Paper II

Outflows in $z \sim 6$ quasars

F. Stanley, J-B. Jolly, S. König, K. K. Knudsen

Submitted to Astronomy & Astrophysics